NASA/CR—1999-208881

PWA 6420–108

Eigenmodes of Ducted Flows With Radially-Dependent Axial and Swirl Velocity Components

Kenneth A. Kousen
United Technologies Corporation, East Hartford, Connecticut

Prepared under Contract NAS3–26618

National Aeronautics and
Space Administration

Glenn Research Center

March 1999

Acknowledgments

The author would like to acknowledge the considerable contributions and help received from Professor David Gottlieb and his students at Brown University. In addition, the author would like to thank Dr. Marvin Goldstein and Dr. David Wundrow of NASA Lewis Research Center (presently NASA Glenn Research Center) for their assistance, and Dr. Choon Tan of MIT for his help. The author would also like to thank Dr. Donald Hanson and Mr. David Topol of Pratt & Whitney Aircraft and Dr. Harold Meyer of Hamilton Standard, and Dr. Joseph Verdon of United Technologies Research Center for many fruitful discussions during this project.

Available from

NASA Center for Aerospace Information
7121 Standard Drive
Hanover, MD 21076
Price Code: A03

National Technical Information Service
5285 Port Royal Road
Springfield, VA 22100
Price Code: A03

Eigenmode Analysis of Ducted Flows With Radially-Dependent Axial and Swirl Velocity Components

Contents

List of Symbols

Roman

A	mean flow speed of sound
A_T	speed of sound at the tip radius
$\bar{A}$	dimensionless speed of sound, A/A_T
D/Dt	convective derivative operator based on mean flow velocity
D_N	derivative matrix using N points
$\mathbf{e}_x, \mathbf{e}_\theta$	unit vector in axial and tangential directions
k_x	perturbation axial wavenumber
k	reduced frequency, $\omega r_T/A_T$
m	number of nodal diameters
M_x, M_θ	axial and tangential Mach number
P, p	mean and perturbation pressure
r	radial coordinate
r_H, r_T	hub and tip radius
$\bar{r}$	dimensionless radial coordinate, r/r_T
S, s	mean and perturbation entropy
t	time
T_k	kth Chebyshev polynomial
$\mathbf{V}$	mean flow velocity
V_θ, V_x	tangential and axial components of mean flow velocity
$\tilde{\mathbf{v}}, \mathbf{v}$	perturbation velocity and its complex amplitude
v_r, v_θ, v_x	radial, tangential, and axial components of perturbation velocity
$\bar{v}_r, \bar{v}_\theta, \bar{v}_x$	perturbation velocity components divided by mean flow speed of sound
v_ϕ	phase velocity, $\bar{k}/\bar{\gamma}$
v_g	group velocity, $d\bar{k}/d\bar{\gamma}$
x	axial coordinate

Greek

$\bar{\gamma}$	dimensionless axial wavenumber, $k_x r_T$
Γ	free vortex strength
$\bar{\Gamma}$	$\Gamma/(r_T A_T)$
δ	Kronecker delta
η_H, η_T	hub and tip acoustic liner admittance
θ	circumferential coordinate
κ	ratio of specific heats
$\kappa_{m\mu}$	modal separation constant, (4.1)
λ	eigenvalue, $-i\bar{\gamma}$
μ	radial mode index
$\bar{\rho}, \rho$	mean and perturbation density
σ	hub to tip radius ratio
τ	transformed eigenvalue, (3.12)
Ω	angular frequency for solid body swirl
$\bar{\Omega}$	$\Omega r_T/A_T$
ω	perturbation angular frequency

Eigenmode Analysis of Ducted Flows With Radially-Dependent Axial and Swirl Velocity Components

Summary

This report characterizes the sets of small disturbances possible in cylindrical and annular ducts with mean flow whose axial and tangential components vary arbitrarily with radius. The linearized equations of motion are presented and discussed, and then exponential forms for the axial, circumferential, and time dependencies of any unsteady disturbances are assumed. The resultant equations form a generalized eigenvalue problem, the solution of which yields the axial wavenumbers and radial mode shapes of the unsteady disturbances. Two numerical discretizations are applied to the system of equations: (1) a spectral collocation technique based on Chebyshev polynomial expansions on the Gauss-Lobatto points, and (2) second and fourth order finite differences on uniform grids. The discretized equations are solved using a standard eigensystem package employing the QR algorithm.

The eigenvalues fall into two primary categories: a discrete set (analogous to the acoustic modes found in uniform mean flows) and a continuous band (analogous to convected disturbances in uniform mean flows) where the phase velocities of the disturbances correspond to the local mean flow velocities. Sample mode shapes and eigensystem distributions are presented for both sheared axial and swirling flows.

The physics of swirling flows is examined with reference to hydrodynamic stability and completeness of the eigensystem expansions. The effect of assuming exponential dependence in the axial direction is discussed.

1. Introduction

Our understanding of ducted, unsteady turbomachinery flows depends to a considerable extent on understanding the behavior of small disturbances in the fluid. For uniform mean flows, these disturbances can be classified as vortical and entropic waves, which are purely convected by the mean flow, and acoustic waves, which either propagate unattenuated or decay exponentially away from their source of origin [1]. The response to any arbitrary unsteady excitation can then be determined as a linear combination of responses due to the entropic, vortical, and acoustic parts of the excitation.

For uniform mean flows, the acoustic disturbances in an annular or cylindrical duct can be described in terms of individual modes [2]. The modes have exponential dependencies in time and in the axial and circumferential directions. The radial behavior is then described in terms of Bessel functions of the first and second kind. The propagation characteristics of the acoustic modes are dependent upon the mean flow quantities, duct geometry, and unsteady excitation parameters. By an appropriate selection of these quantities, undesired acoustic modes can be "cut off," i.e., generated such that they decay exponentially as they move in the axial direction.

The unsteady modes also serve as means of communication between acoustic elements in a turbomachine [3, 4], and can be used to determine the coupled responses of several acoustic elements simultaneously[5]. In addition, the derivation of so-called "non-reflecting" far-field boundary conditions for CFD analyses depends on an accurate modeling of the far-field unsteady behavior, otherwise the inlet and exit boundaries will give rise to spurious, non-physical reflections [1, 6, 7].

The behavior of unsteady perturbations in ducted, uniform axial mean flows can be described by a convected wave equation. For uniform mean flows, this equation is separable into the dependencies listed above. To determine the analogous behavior for nonuniform mean flows, the assumption of periodic behavior in time and in the axial and tangential directions results in a linear second-order ordinary differential equation for the radial behavior. This equation, while linear, has variable coefficients, and does not permit an analytic solution. It also contains a separation constant, arising in the separation of variables solution of the convected wave equation, that acts as the eigenvalue for the unsteady acoustic modes. Numerical efforts to determine the modes require a discretization in the radial direction and a subsequent calculation of the eigenvalues and eigenvectors of the discretized system.

Early work in the modal analysis of nonuniform mean flows concentrated on integrating the second-order ODE for the radial behavior, generally through numerical means. In the cases of flows with mean axial shear, the relevant ODE was first analyzed for two-dimensional flows by Pridmore-Brown [8]. Subsequent investigators integrated the ODE using Runge-Kutta methods [9, 10], iterative methods [11], and Galerkin based methods [12]. See [13] for a review up to 1975. Since that time, numerical work has been done in [14] and [15], and a theoretical basis for shear flows is given in [16, 17].

Less attention has been focussed on ducted, compressible swirling flows in turbomachinery, although there is a rich literature [18] concerning rotating incompressible fluids without axial flow components. The linearized Euler equations for flows with swirl are presented in [19, 20, 21], and cases with solid body swirl have been examined in [22, 23] and [24]. Finally, Wundrow in [25] has examined swirling potential flows, i.e., flows containing a free vortex swirl. The swirling flow results have been applied to special classes of flows, such as solid body and free vortex swirl. This restriction is relaxed in the present analysis.

While it is intuitively reasonable to assume that the unsteady behavior in time and the circumferential direction can be described by exponentials, it is not as clear that this is an appropriate assumption for the axial direction. There are thus significant existence, uniqueness, and completeness questions regarding the analysis. These questions have been addressed to some degree by Shankar [26, 10] and Swinbanks [27], who suggest that completeness may be achievable. Goldstein [16, 17] described the complete solution for transversely sheared mean flows, and demonstrated the existence of a continuum of eigenvalues, some of which give rise to acoustic disturbances and some of which do not. These two categories of disturbances are discussed to some degree below. It is notable that Case [28, 29] specifically warned against the "naive" approach of assuming exponential behavior, which could potentially miss the continuum modes. He recommended that the linearized equations be solved using Fourier and Laplace transforms. In doing so, the continua of eigenvalues arise naturally. Perhaps even more interesting is the fact that, according to Case [28], the same continuum was first observed by Rayleigh [30] in 1913.

In this report, the flow inside a constant radius annular or cylindrical duct with acoustically lined walls is examined using the linearized unsteady Euler equations. Any unsteady disturbances are presumed to have

exponential dependence in the axial and circumferential directions as well as time. The radial behavior is then found by discretizing the equations on a Chebyshev-Gauss-Lobatto grid and analyzing the discrete system using a standard eigensystem package. In the nonuniform mean flows studied, the unsteady disturbances fall into two groups: a discrete set analogous to the acoustic modes in uniform mean flows and a continuous band of "convected" modes.

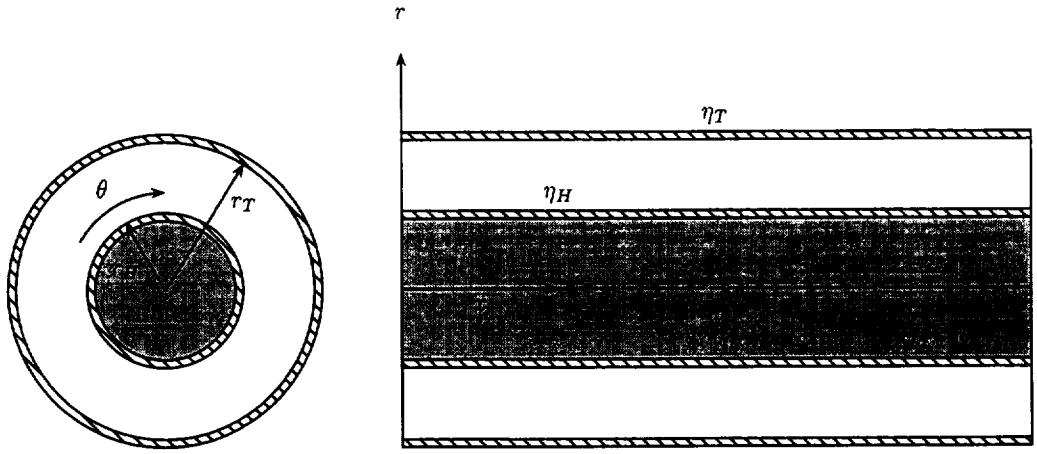

Figure 2.1: Annular duct geometry.

2. Aerodynamic Model

The physical system consists of a cylindrical or annular duct (see Fig.2.1) with or without acoustically lined walls. It is assumed throughout this section that the mean flow is isentropic, the steady velocity has no radial component, and that all mean flow quantities are at most dependent upon radial position. The governing equations are the unsteady Euler equations, which can be linearized about a nonlinear mean flow.

2.1 Mean Flow

The mean flow (and therefore not time-dependent) entropy, momentum, and continuity equations are

$$\nabla S = 0 \tag{2.1}$$

$$(\mathbf{V}\cdot\nabla)\mathbf{V} = -\bar{\rho}^{-1}\nabla P \tag{2.2}$$

and

$$\nabla\cdot(\mathbf{V}\bar{\rho}) = 0 \tag{2.3}$$

where $S, \mathbf{V}, P$, and $\bar{\rho}$ represent the entropy, velocity, pressure, and density in the mean flow.

The mean flow is taken to be isentropic and axisymmetric, so that it has the general form

$$\mathbf{V}(r,\theta,x) = V_x(r)\mathbf{e}_x + V_\theta(r)\mathbf{e}_\theta \tag{2.4}$$

where $\mathbf{e}_x$ and $\mathbf{e}_\theta$ are unit vectors in the axial and circumferential directions, respectively.

In addition to handling general mean flows satisfying (2.4), several special flow cases are examined in the Results section below. Chief among these are (a) axial shear flow, (b) solid body swirl, and (c) free vortex swirl. Mean flows containing only axial shear, i.e., $\mathbf{V} = V_x(r)\mathbf{e}_x$, have been examined by many authors and are thus used for validation of the present analysis. For such mean flows, the mean pressure, density, and, therefore, speed of sound, are all constant across the duct.

If the mean flow contains a swirl component, the mean pressure, mean density, and mean speed of sound are no longer uniform. Integration of the radial momentum equation leads to

$$P = \int_{\bar{r}}^{1} \frac{\bar{\rho}V_\theta^2}{\bar{r}}\, d\bar{r} \tag{2.5}$$

where $\bar{r}$ is the radial coordinate normalized by the tip diameter r_T. Thus the reference point is the duct location, $\bar{r} = 1$. The isentropic condition $\nabla S = 0$ implies that $\nabla P = A^2\nabla\bar{\rho}$ and is used to determine the mean flow density. With swirl, the mean flow speed of sound can be determined from $A^2 = \kappa P/\bar{\rho}$ where κ

is the ratio of specific heats. Defining $\bar{A} = A(r)/A(1) = A(r)/A_T$ where A_T is the speed of sound at the tip implies that

$$\bar{A}(r) = \exp\left(\frac{1-\kappa}{2}\int_{\bar{r}}^{1}\frac{M_\theta^2}{\bar{r}}\,d\bar{r}\right) \tag{2.6}$$

For the special cases of solid body and free vortex swirl, it is easier to determine $\bar{A}$ by taking the derivative of $A^2 = \kappa P/\bar{\rho}$ and substituting in the expressions for P and $\bar{\rho}$ given above. This produces

$$\frac{dA}{dr} = \frac{(\kappa-1)V_\theta^2}{2rA} \tag{2.7}$$

whose solution is

$$A^2(r) = A_T^2 - (\kappa-1)\int_r^{r_T}\frac{V_\theta^2}{r}\,dr \tag{2.8}$$

which is normalized by A_T subsequently. For solid body swirl, free vortex swirl, and the two together, the tangential velocity is given by

$$V_{\theta,\mathrm{sb}} = \Omega r \tag{2.9}$$

$$V_{\theta,\mathrm{fv}} = \frac{\Gamma}{r} \tag{2.10}$$

$$V_{\theta,\mathrm{sb,fv}} = \Omega r + \frac{\Gamma}{r} \tag{2.11}$$

and the normalized speed of sound $\bar{A}$ is found to be

$$\bar{A}^2_{\mathrm{sb}}(\bar{r}) = 1 - \left(\frac{\kappa-1}{2}\right)\bar{\Omega}^2(1-\bar{r}^2) \tag{2.12}$$

$$\bar{A}^2_{\mathrm{fv}}(\bar{r}) = 1 - \left(\frac{\kappa-1}{2}\right)\bar{\Gamma}^2\left(\frac{1}{\bar{r}^2}-1\right) \tag{2.13}$$

$$\bar{A}^2_{\mathrm{sb,fv}}(\bar{r}) = 1 - \left(\frac{\kappa-1}{2}\right)\left[\bar{\Omega}^2(1-\bar{r}^2) - \bar{\Gamma}^2\left(1-\frac{1}{\bar{r}^2}\right)\right] + 2(\kappa-1)\bar{\Omega}\bar{\Gamma}\log\bar{r} \tag{2.14}$$

where $\bar{\Omega} = \Omega r_T/A_T$ and $\bar{\Gamma} = \Gamma/(r_T A_T)$.

Note that Crocco's theorem implies that for an irrotational flow (which requires V_x = constant and $V_\theta = \Gamma/r$) the stagnation enthalpy is a constant, so the ratio $\bar{A}(r_1)/\bar{A}(r_2)$ can be calculated from the isentropic flow relations between any two radial locations r_1 and r_2. The mean flow is assumed to be isentropic, so the mean flow pressure and density can be expressed in terms of $\bar{A}$ as

$$\bar{\rho}(\bar{r}) = \bar{A}^{2/(\kappa-1)}, \quad \text{and} \quad \bar{P}(\bar{r}) = \bar{A}^{4/(\kappa-1)} \tag{2.15}$$

where the pressure, density, speed of sound, and radius have all been nondimensionalized by their values at the tip radius, r_T.

According to Kerrebrock [20, 21], solid body swirl can be used to represent the flow in a behind a high-work blade row, and adding free vortex swirl models the flow behind a rotor. The case of purely free vortex swirl is also of particular interest, since it is irrotational and can thus be analyzed using the considerable machinery developed for potential flows [31, 25].

2.2 Unsteady Flow

The first order unsteady entropy, momentum, and continuity equations are

$$\frac{\bar{D}\tilde{s}}{Dt} = 0 \tag{2.16}$$

$$\frac{\bar{D}\tilde{\mathbf{v}}}{Dt} - \tilde{s}(\mathbf{V}\cdot\boldsymbol{\nabla})\mathbf{V} + (\tilde{\mathbf{v}}\cdot\boldsymbol{\nabla})\mathbf{V} = -\boldsymbol{\nabla}(\bar{\rho}^{-1}\tilde{p}) \tag{2.17}$$

and

$$\frac{\bar{D}\tilde{p}}{Dt} + A^2(\tilde{\mathbf{v}}\cdot\boldsymbol{\nabla})\bar{\rho} \quad + \quad \bar{\rho}A^2\boldsymbol{\nabla}\cdot\tilde{\mathbf{v}} = 0 \tag{2.18}$$

where $\bar{D}/Dt$ is the convective derivative operator following the mean flow and tildes indicate perturbation quantities. The present analysis assumes isentropic flow, so $\tilde{s} = 0$ which implies $\tilde{p} = A^2\tilde{\rho}$.

Axial shear flows

In an axial shear flow, the governing equations (2.17,2.18) can be expressed in cylindrical coordinates as

$$\frac{\partial\tilde{v}_r}{\partial t} + V_x\frac{\partial\tilde{v}_r}{\partial x} = -\frac{1}{\bar{\rho}}\frac{\partial\tilde{p}}{\partial r} \tag{2.19}$$

$$\frac{\partial\tilde{v}_\theta}{\partial t} + V_x\frac{\partial\tilde{v}_\theta}{\partial x} = -\frac{1}{\bar{\rho}r}\frac{\partial\tilde{p}}{\partial\theta} \tag{2.20}$$

$$\frac{\partial\tilde{v}_x}{\partial t} + V_x\frac{\partial\tilde{v}_x}{\partial x} + V_x'\tilde{v}_r = -\frac{1}{\bar{\rho}}\frac{\partial\tilde{p}}{\partial x} \tag{2.21}$$

$$\frac{1}{\bar{\rho}A^2}\left(\frac{\partial\tilde{p}}{\partial t} + V_x\frac{\partial\tilde{p}}{\partial x}\right) \quad + \quad \frac{\partial\tilde{v}_r}{\partial r} + \frac{\tilde{v}_r}{r} + \frac{1}{r}\frac{\partial\tilde{v}_\theta}{\partial\theta} + \frac{\partial\tilde{v}_x}{\partial x} = 0 \tag{2.22}$$

If one then assumes that the perturbation quantities $\tilde{p}, \tilde{v}_r, \tilde{v}_\theta$, and $\tilde{v}_x$ all have the exponential dependence

$$\tilde{f}(r,\theta,x,t) = f(r)e^{i(k_x x + m\theta - \omega t)} \tag{2.23}$$

for $f = p, v_r, v_\theta, v_x$, then the velocity components can be expressed in terms of the pressure and its derivative via

$$\bar{v}_r = \frac{-i}{(k - M_x\bar{\gamma})}\frac{d\bar{p}}{d\bar{r}} \tag{2.24}$$

$$\bar{v}_\theta = \frac{m}{\bar{r}\,(k - M_x\bar{\gamma})}\bar{p} \tag{2.25}$$

$$\bar{v}_x = \frac{-M_x}{(k - M_x\bar{\gamma})^2}\frac{d\bar{p}}{d\bar{r}} + \frac{\bar{\gamma}}{(k - M_x\bar{\gamma})}\bar{p} \tag{2.26}$$

where $k = \omega r_T/A_T$ and $\bar{\gamma} = k_x r_T$. When substituted into the continuity equation, these give

$$\frac{d^2\bar{p}}{d\bar{r}^2} + \left[\frac{1}{\bar{r}} - \frac{2M_x'\bar{\gamma}}{(k - M_x\bar{\gamma})}\right]\frac{d\bar{p}}{d\bar{r}} + \left[(k - M_x\bar{\gamma})^2 - \frac{m^2}{\bar{r}^2} - \bar{\gamma}^2\right]\bar{p} = 0 \tag{2.27}$$

as the second order ODE for the pressure.

Previous attempts to determine the radial behavior of the unsteady quantities in an axial shear flow concentrated on solving this ODE numerically. This was examined in the present work, and is discussed in Section 3.5 below, it should be mentioned that this approach can miss entire families of perturbations. As illustrated in Goldstein [32], the linearized momentum and continuity partial differential equations governing the behavior of parallel shear flows can be combined into a single partial differential equation by taking the divergence of the momentum equation and subtracting the material derivative of the continuity equation, to get

$$\frac{1}{A^2}\frac{D^2\tilde{p}}{Dt^2} - \boldsymbol{\nabla}^2\tilde{p} = 2\bar{\rho}V_x'\frac{\partial\tilde{v}_r}{\partial x} \tag{2.28}$$

where V_x' indicates the radial derivative of the axial mean flow velocity. A single equation for pressure can be found by taking the material derivative of both sides and using the radial momentum equation, which gives

$$\frac{1}{A^2}\frac{D^3\tilde{p}}{Dt^3} - \frac{D}{Dt}\left(\boldsymbol{\nabla}^2\tilde{p}\right) + 2V_x'\frac{\partial^2\tilde{p}}{\partial x\partial r} = 0 \tag{2.29}$$

The exponential assumption (2.23) applied to this equation gives

$$(k - M_x\bar{\gamma})\left\{\frac{d^2\bar{p}}{d\bar{r}^2} + \left[\frac{1}{\bar{r}} - \frac{2M_x'\bar{\gamma}}{(k - M_x\bar{\gamma})}\right]\frac{d\bar{p}}{d\bar{r}} + \left[(k - M_x\bar{\gamma})^2 - \frac{m^2}{\bar{r}^2} - \bar{\gamma}^2\right]\bar{p}\right\} = 0 \tag{2.30}$$

Case [28, 29] and Goldstein [16, 17] each point out that equations of the form

$$xf(x) = 0 \tag{2.31}$$

where $f(x)$ is a differential operator have as solutions $x = 0$, $f(x) = 0$, and $f(x) = \delta(x)$, where δ is the Kronecker delta. In the case of (2.30), this becomes

$$\bar{\lambda} L[\bar{p}] = 0 \tag{2.32}$$

where $\bar{\lambda} = k - \bar{\gamma} M_x$ and $L[\bar{p}]$ represents the second order ODE for pressure. There are thus three sets of solutions to the shear flow eigenvalue problem: (1) the case $\bar{\lambda}(\bar{r}) = 0$ everywhere across the duct, which gives rise to a continuum of disturbances; (2) the case $L[\bar{p}(\bar{r})] = 0$, which produces a discrete set of eigenvalues $\bar{\gamma}_k$ arising from the ODE; and (3) the case $L[\bar{p}(\bar{r})] = \delta(\bar{\lambda} = 0)$, which also consists of a continuum of eigenvalues. The circumferential momentum equation with the exponential assumption reduces to $\bar{\lambda} v_\theta = -im/(\bar{\rho} r) p$, indicating that the disturbances in set (1) have no pressure associated with them. Set (2) are the wavenumbers analogous to the discrete acoustic disturbances in uniform axial flow. The right hand side of the condition in set (3) is nonzero only at points where the phase velocity of the disturbance $v_\phi = k/\bar{\gamma} = M_x$ in the duct. This latter set acts as a source for unsteady acoustic disturbances in the flow.

Flows with mean axial shear and swirl

The linearized perturbation equations for swirling flows in cylindrical coordinates are

$$\frac{\partial \tilde{v}_r}{\partial t} + \frac{V_\theta}{r}\frac{\partial \tilde{v}_r}{\partial \theta} + V_x \frac{\partial \tilde{v}_r}{\partial x} - \frac{2V_\theta}{r}\tilde{v}_\theta = -\frac{1}{\bar{\rho}}\frac{\partial \tilde{p}}{\partial r} + \frac{V_\theta^2}{\bar{\rho} r A^2}\tilde{p} \tag{2.33}$$

$$\frac{\partial \tilde{v}_\theta}{\partial t} + \frac{V_\theta}{r}\frac{\partial \tilde{v}_\theta}{\partial \theta} + V_x \frac{\partial \tilde{v}_\theta}{\partial x} + \left(\frac{V_\theta}{r} + \frac{dV_\theta}{dr}\right)\tilde{v}_r = -\frac{1}{\bar{\rho} r}\frac{\partial \tilde{p}}{\partial \theta} \tag{2.34}$$

$$\frac{\partial \tilde{v}_x}{\partial t} + \frac{V_\theta}{r}\frac{\partial \tilde{v}_x}{\partial \theta} + V_x \frac{\partial \tilde{v}_x}{\partial x} + \frac{dV_x}{dr}\tilde{v}_r = -\frac{1}{\bar{\rho}}\frac{\partial \tilde{p}}{\partial x} \tag{2.35}$$

$$\frac{1}{\bar{\rho} A^2}\left(\frac{\partial \tilde{p}}{\partial t} + \frac{V_\theta}{r}\frac{\partial \tilde{p}}{\partial \theta} + V_x \frac{\partial \tilde{p}}{\partial x}\right) + \frac{V_\theta^2}{r A^2}\tilde{v}_r + \frac{\partial \tilde{v}_r}{\partial r} + \frac{\tilde{v}_r}{r} + \frac{1}{r}\frac{\partial \tilde{v}_\theta}{\partial \theta} + \frac{\partial \tilde{v}_x}{\partial x} = 0 \tag{2.36}$$

where $A(r)$ is the local speed of sound in the mean flow.

The same procedure that resulted in a single partial differential equation for axial shear can be applied to the swirl flow equations, but the results are not as satisfactory. Subtracting the material derivative of the continuity equation from the divergence of the momentum equation gives

$$\frac{D}{Dt}\left(\frac{1}{\bar{\rho} A^2}\frac{D\tilde{p}}{Dt}\right) - \nabla^2\left(\frac{\tilde{p}}{\bar{\rho}}\right) = -\frac{D}{Dt}\left(\frac{V_\theta^2}{r A^2}\tilde{v}_r\right) + 2\frac{dV_x}{dr}\left(\frac{\partial \tilde{v}_r}{\partial x} + \frac{1}{r}\frac{\partial \tilde{v}_r}{\partial \theta}\right) - \frac{2}{r}\left(V_\theta \frac{\partial \tilde{v}_\theta}{\partial r} + \frac{dV_\theta}{dr}\tilde{v}_\theta\right) \tag{2.37}$$

Unlike the shear flow case, it is does not appear that going to higher order here can result in a single equation for $\tilde{p}$. In view of the simplicity of the discretized first-order system technique detailed below, the general PDE has not been pursued.

After substituting in the exponential form (2.23) and using $M_x = V_x/A$, $M_\theta = V_\theta/A$, $\bar{v}_r = v_r/A$, $\bar{v}_\theta = v_\theta/A$, $\bar{v}_x = v_x/A$, and $\bar{p} = p/(\bar{\rho} A^2)$, the linearized equations become

$$i\left(\frac{k}{\bar{A}} - \frac{m}{\bar{r}}M_\theta - \bar{\gamma} M_x\right)\bar{v}_r + \frac{2}{\bar{r}}M_\theta \bar{v}_\theta = \frac{d\bar{p}}{d\bar{r}} + \frac{(\kappa - 1)}{\bar{r}}M_\theta^2 \bar{p} \tag{2.38}$$

$$-i\left(\frac{k}{\bar{A}} - \frac{m}{\bar{r}}M_\theta - \bar{\gamma} M_x\right)\bar{v}_\theta + \left[\frac{M_\theta}{\bar{r}} + \frac{dM_\theta}{d\bar{r}} + \frac{(\kappa - 1)}{2\bar{r}}M_\theta^3\right]\bar{v}_r = -\frac{im}{\bar{r}}\bar{p} \tag{2.39}$$

$$-i\left(\frac{k}{\bar{A}} - \frac{m}{\bar{r}}M_\theta - \bar{\gamma} M_x\right)\bar{v}_x + \left[\frac{dM_x}{d\bar{r}} + \frac{(\kappa - 1)}{2\bar{r}}M_x M_\theta^2\right]\bar{v}_r = -i\bar{\gamma}\bar{p} \tag{2.40}$$

$$-i\left(\frac{k}{\bar{A}} - \frac{m}{\bar{r}}M_\theta - \bar{\gamma} M_x\right)\bar{p} + \frac{d\bar{v}_r}{d\bar{r}} + \left[\frac{(\kappa + 1)}{2\bar{r}}M_\theta^2 + \frac{1}{\bar{r}}\right]\bar{v}_r + \frac{im}{\bar{r}}\bar{v}_\theta + i\bar{\gamma}\bar{v}_x = 0 \tag{2.41}$$

where the mean flow relationships

$$\frac{1}{\bar{A}}\frac{d\bar{A}}{d\bar{r}} = \frac{(\kappa-1)M_\theta^2}{2\bar{r}} \tag{2.42}$$

$$\frac{1}{\bar{\rho}}\frac{d\bar{\rho}}{d\bar{r}} = \frac{M_\theta^2}{\bar{r}} \tag{2.43}$$

have been used. Letting

$$\bar{\lambda} = \frac{k}{\bar{A}} - \frac{m}{\bar{r}}M_\theta - \bar{\gamma}M_x \tag{2.44}$$

$$\mu = \frac{M_\theta}{\bar{r}} + \frac{dM_\theta}{d\bar{r}} + \frac{\kappa-1}{2}\frac{M_\theta^3}{\bar{r}} \tag{2.45}$$

$$\nu = -\lambda^2 + \frac{2}{\bar{r}}M_\theta\mu \tag{2.46}$$

then results in expressions for the perturbation velocity components in terms of the pressure and its radial derivative

$$\bar{v}_r = \frac{M_\theta}{\nu\bar{r}}\left[-2i\frac{m}{\bar{r}} + (\kappa-1)\bar{\lambda}M_\theta\right]p + i\frac{\bar{\lambda}}{\nu}\frac{dp}{dr} \tag{2.47}$$

$$\bar{v}_\theta = \left[-\frac{m\bar{\lambda}}{r\nu} + \frac{\kappa-1}{2}\left(1+\frac{\bar{\lambda}^2}{\nu}\right)M_\theta\right]p + \frac{\bar{r}}{2M_\theta}\left(1+\frac{\bar{\lambda}^2}{\nu}\right)\frac{dp}{dr} \tag{2.48}$$

$$\begin{aligned}\bar{v}_x = {} & \left[\frac{\bar{\gamma}}{\bar{\lambda}} + \frac{(1-\kappa)M_\theta^3 M_x}{\bar{\lambda}\nu\bar{r}^3}\left(1+\frac{1-\kappa}{2}M_\theta\bar{\lambda}\bar{r}\right) + \frac{M_\theta}{\nu\bar{r}}\left(-\frac{2m}{\bar{\lambda}\bar{r}} + (\kappa-1)M_\theta\right)\frac{dM_x}{d\bar{r}}\right]p \\ & + \frac{1}{\nu}\left[\frac{\kappa-1}{2\bar{r}}M_xM_\theta^2 + 1\right]\frac{dp}{d\bar{r}}\end{aligned} \tag{2.49}$$

The ODE for pressure then becomes

$$\begin{aligned}&\frac{d^2p}{d\bar{r}^2} + \left\{\frac{1}{\bar{r}} + \frac{m(\nu+\bar{\lambda}^2)}{2\bar{\lambda}M_\theta} + \frac{(1+\kappa)M_\theta^2}{2\bar{r}} - \frac{iM_\theta}{\bar{\lambda}\bar{r}}\left[(\kappa-1)\bar{\lambda}M_\theta - \frac{2im}{\bar{r}}\right] + \frac{\bar{\gamma}}{\bar{\lambda}}\left[\frac{(\kappa-1)M_xM_\theta^2}{2\bar{r}} + \frac{dM_x}{d\bar{r}}\right]\right\}\frac{dp}{d\bar{r}} \\ &+ \left\{-\frac{i}{\bar{\lambda}\bar{r}}\left[\bar{\lambda}(\kappa-1)M_\theta - \frac{2im}{\bar{r}}\right]\left[\frac{(1+\kappa)M_\theta^3}{2\bar{r}} + \frac{dM_\theta}{d\bar{r}}\right] + \frac{\kappa-1}{2}\left(1+\frac{\bar{\lambda}^2}{\nu}\right)\frac{m\nu M_\theta}{\bar{\lambda}\bar{r}}\right. \\ &+ \frac{iM_\theta}{\bar{\lambda}\bar{r}}\left[\frac{2im}{\bar{r}^2} + (\kappa-1)\bar{\lambda}\frac{dM_\theta}{d\bar{r}}\right] - \frac{m^2}{\bar{r}^2} + \frac{\bar{\gamma}^2}{\bar{\lambda}} + \frac{\bar{\gamma}}{\bar{\lambda}}\left[\frac{(1-\kappa)M_\theta^3M_x}{\bar{\lambda}\bar{r}^3} + \frac{(1-\kappa)^2M_\theta^4M_x}{2\bar{r}^2}\right. \\ &+ \left.\left.\frac{M_\theta}{\bar{r}}\left((\kappa-1)M_\theta\frac{dM_x}{d\bar{r}} - \frac{2m}{\bar{\lambda}\bar{r}}\right)\right]\right\}p = 0\end{aligned} \tag{2.50}$$

The linearized perturbation equations can thus be written in matrix form as

$$\mathbf{Ax} = \lambda\mathbf{Bx} \tag{2.51}$$

where

$$\mathbf{A} = \begin{bmatrix} -i\left(\frac{k}{\bar{A}} - \frac{m}{\bar{r}}M_\theta\right) & -\frac{2}{\bar{r}}M_\theta & 0 & \frac{d}{d\bar{r}} + \frac{(\kappa-1)}{\bar{r}}M_\theta^2 \\ \frac{1}{\bar{r}}M_\theta + \frac{dM_\theta}{d\bar{r}} + \frac{(\kappa-1)}{2\bar{r}}M_\theta^3 & -i\left(\frac{k}{\bar{A}} - \frac{m}{\bar{r}}M_\theta\right) & 0 & i\frac{m}{\bar{r}} \\ \frac{dM_x}{d\bar{r}} + \frac{(\kappa-1)}{2\bar{r}}M_xM_\theta^2 & 0 & -i\left(\frac{k}{\bar{A}} - \frac{m}{\bar{r}}M_\theta\right) & 0 \\ \frac{d}{d\bar{r}} + \frac{1}{\bar{r}} + \frac{(\kappa+1)}{2\bar{r}}M_\theta^2 & i\frac{m}{\bar{r}} & 0 & -i\left(\frac{k}{\bar{A}} - \frac{m}{\bar{r}}M_\theta\right) \end{bmatrix} \tag{2.52}$$

$$\mathbf{B} = \begin{bmatrix} M_x & 0 & 0 & 0 \\ 0 & M_x & 0 & 0 \\ 0 & 0 & M_x & 1 \\ 0 & 0 & 1 & M_x \end{bmatrix}, \quad \mathbf{x} = \begin{Bmatrix} \bar{v}_r \\ \bar{v}_\theta \\ \bar{v}_x \\ \bar{p} \end{Bmatrix}, \quad \text{and} \quad \lambda = -i\bar{\gamma} \tag{2.53}$$

The matrices **A** and **B** are then dependent only upon the radial coordinate. Note that the radial derivative operator, $d/d\bar{r}$, is retained in the coefficient matrices.

Matrix **B** in (2.51) has an analytical inverse provided its determinant

$$\det \mathbf{B} = M_x^2(M_x + 1)(M_x - 1) \tag{2.54}$$

is nonzero, Thus **B** is singular whenever $M_x = 0$ or $M_x = \pm 1$ in the flow. If the mean flow is presumed to be subsonic, then the only difficulty that arises is when a boundary layer profile is specified and the mean flow Mach number is zero at the wall(s). If **B** is nonsingular, the generalized eigenvalue problem (2.51) can be reduced to a standard eigenvalue problem using the analytical inverse of **B**. Singularity of **B** does not imply that the generalized eigenvalue problem (2.51) cannot be solved, but it would complicate the solution of the eigenvalue problem $\mathbf{B}^{-1}\mathbf{A}\mathbf{x} = \lambda\mathbf{x}$. Consequently, the numerical algorithm is kept in the generalized eigensystem form.

Note also that there are several terms in the **A** and **B** matrices that are singular at $\bar{r} = 0$, i.e., in the case of a hollow cylinder. In the analysis, these terms are evaluated by using l'Hôpital's rule as $\bar{r} \to 0$.

2.3 Boundary Conditions

The hard wall boundary conditions applied to the system come from the requirement that there be no flow into the walls, i.e.,

$$\bar{v}_r(\sigma) = \bar{v}_r(1) = 0\,. \tag{2.55}$$

where $\sigma = r_H/r_T$ is the hub-to-tip radius ratio for the duct.

For acoustically lined ducts, the wall boundary condition used by Unruh and Eversman [12] in sheared axial flows is

$$\bar{v}_r(1) = \eta_T \left[1 - \frac{\bar{\gamma}}{k} M(1)\right] \bar{p}(1) \tag{2.56}$$

$$\bar{v}_r(\sigma) = \eta_H \left[1 - \frac{\bar{\gamma}}{k} M(\sigma)\right] \bar{p}(\sigma) \tag{2.57}$$

where η_T and η_H are the complex admittances of the liners along the outer and inner duct walls and $M(1) = \sqrt{M_x^2(1) + M_\theta^2(1)}$ and $M(\sigma) = \sqrt{M_x^2(\sigma) + M_\theta^2(\sigma)}$ are the local Mach numbers at those locations. These liner boundary conditions are based on the continuity of particle displacement. It will be presumed in this report that the same liner boundary conditions can be used in more general, swirling flows, provided the correct local Mach numbers are used.

3. Numerical Methods

The system of equations (2.51) is in the form of a nonhermetian generalized eigenvalue problem. The eigenvalues are related to the axial wavenumbers of any unsteady disturbances via $\lambda = -i\gamma$, and the eigenvectors contain the radial behavior of v_r, v_θ, v_x, and p. In order to determine the eigenvalues and eigenvectors, it is necessary to discretize the equations in the radial direction. Two categories of discretizations have been implemented: a spectral technique based on the Chebyshev-Gauss-Lobatto points and a finite difference method using both second and fourth order differences. Each case will be presented in turn.

3.1 Spectral derivative matrix

For any discretization, a derivative matrix is required, such that

$$D_N f(x_j) = \frac{df_j}{dx} \tag{3.1}$$

for an arbitrary discretized function $f_j = f(x_j)$. The spectral grid uses the Chebyshev-Gauss-Lobatto points [33], which satisfy

$$x_j = \cos\frac{\pi j}{N}, \quad j = 0, \ldots, N \tag{3.2}$$

and are the extrema of the Nth order Chebyshev polynomial

$$T_N(x) = \cos\left(N \cos^{-1} x\right). \tag{3.3}$$

Let $f(x)$ be a smooth function of x on the interval $[-1, 1]$. Then $f(x)$ is interpolated by constructing the Nth order interpolation polynomial $g_j(x)$ such that $g_j(x_k) = \delta_{jk}$, and

$$h(x) = \sum_{j=0}^{N} h_j g_j(x) \tag{3.4}$$

where $h(x)$ is the polynomial of degree N and $h_j = f(x_j), j = 0, \ldots, N$. It can be shown that

$$g_j(x) = \frac{(-1)^{j+1}(1-x^2)T_N'(x)}{\bar{c}_j N^2 (x - x_j)}, \; j = 0, \ldots, N \tag{3.5}$$

where

$$\bar{c}_j = \begin{cases} 2 & j = 0, N \\ 1 & 1 \le j \le N-1 \end{cases} \tag{3.6}$$

The derivative of $f(x)$ at the collocation points is then computed by taking the analytic derivative of $g_j(x)$ and evaluating it at the collocation points, which produces $(D_N)_{kj} = g_j'(x_k)$ where

$$(D_N)_{lj} = \begin{cases} \dfrac{\bar{c}_l(-1)^{l+j}}{\bar{c}_j(x_l - x_j)} & l \neq j \\ \dfrac{-x_j}{2(1-x_j^2)} & 1 \le l = j \le \dfrac{N}{2} \\ \dfrac{2N^2+1}{6} & l = j = 1 \\ -\dfrac{2N^2+1}{6} & l = j = N \end{cases} \tag{3.7}$$

is the required derivative matrix [33]. It is shown in [34] that the most accurate method of formulating this matrix is to use

$$(D_N)_{lj} = \begin{cases} \dfrac{-\bar{c}_l(-1)^{l+j}}{2\bar{c}_j \sin\frac{\pi}{2N}(k+j)\sin\frac{\pi}{2N}(k-j)} & l \neq j \\ \dfrac{-\cos(\frac{\pi}{N}l)}{2\sin^2(\frac{\pi}{N}l)} & 1 \leq l = j \leq N-1 \\ \dfrac{2N^2+1}{6} & l = j = 1 \end{cases} \tag{3.8}$$

for $l = 1, \ldots, N/2$, $j = 1, \ldots, N$ and then use

$$(D_N)_{lj} = -(D_N)_{N-l,N-j}, \quad l = \frac{N}{2}+1, \ldots, N \tag{3.9}$$

for the rest of the matrix.

A further improvement on this technique is given in [35]. The idea there is to transform the grid such that

$$\xi = s(x,\alpha) = \frac{\sin^{-1}(\alpha x)}{\sin^{-1}\alpha} \tag{3.10}$$

where α is a parameter, so that the derivative of the function $f(x)$ is now given by

$$\frac{df}{d\xi} = \frac{df}{dx}\frac{dx}{d\xi} \tag{3.11}$$

where

$$\frac{dx}{d\xi} = \frac{1}{s'(x,\alpha)} = \frac{\sin^{-1}\alpha}{\alpha}\sqrt{1-(\alpha x)^2}\,. \tag{3.12}$$

Then the derivative of $f(x)$ at the collocation points is given by

$$f'(x) = MD_N f(x) \tag{3.13}$$

where the diagonal matrix M has elements

$$M_{ll} = \frac{1}{s'(x_l,\alpha)}\,. \tag{3.14}$$

The new derivative matrix is then defined to be MD_N, which shall be referred to as D_N. It is shown in [36] that an appropriate choice for α is

$$\alpha = \operatorname{sech}\left(\frac{|\ln\epsilon|}{N}\right) \tag{3.15}$$

where ϵ is roughly machine zero[1]. This has been implemented into the code and yields excellent results. With this modification, less than three points per wavelength are required to resolve a given eigenmode.

The derivative matrix D_N is therefore a full matrix, so any blocks in (2.51) containing d/dr will be full. The remaining blocks are diagonal, where the radial distribution of the quantity is distributed along the diagonal. The resulting eigenvalue problem is complex, nonhermetian, and $4N \times 4N$ where N is the number of grid points in the radial direction.

The Chebyshev-Gauss-Lobatto points (3.2) are shown in Fig. 3.1. The grid points are thus concentrated at the edges of the domain, which is appropriate for mean flows with boundary layers at the walls. Note that the grid points in (3.2) range from $x_0 = 1$ to $x_N = -1$. The grid is reversed in the present analysis, so that the transformation from each system to the other is given by

$$\bar{r} = \frac{1-\sigma}{2}\left(x + \frac{1+\sigma}{1-\sigma}\right) \quad \text{and} \quad x = \frac{2\bar{r}}{1-\sigma} - \left(\frac{1+\sigma}{1-\sigma}\right) \tag{3.16}$$

[1] On the IBM RS6000 that the bulk of the results were run on, double precision machine zero is approximately 1.11×10^{-16}

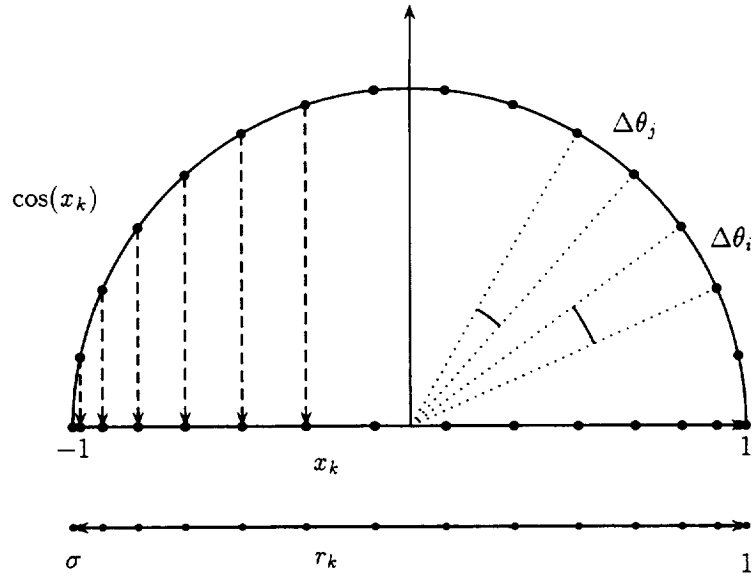

Figure 3.1: Chebyshev-Gauss-Lobatto grid, and mapping from $[-1,1]$ to $[\sigma,1]$. All angles $\Delta\theta_i = \Delta\theta_j$, and the x_j grid points are the cosines of the equally-spaced angles.

The spectral derivative D expressed in Eq. (3.7) was derived based on Lagrangian interpolation polynomials in spectral space, i.e., the range $[-1,1]$. In the present numerical approach, all calculations other than the spectral derivative are done in physical space, so it is easiest to modify D in (2.51) to be

$$D_* = \frac{1-\sigma}{2} D \tag{3.17}$$

which is what is actually implemented in the code.

The solution technique is thus a collocation scheme which requires that the system equations be enforced at each radial station. Application of the boundary conditions (2.55) is done by replacing the equations at $r = \sigma$ and $r = 1$ by the discrete forms of the boundary conditions. Soft-walled boundary conditions modeling the effects of acoustic liners are introduced using a complex admittance coefficient η.

3.2 Finite difference derivative matrix

Second and fourth order finite difference derivative matrices were developed for comparison to the spectral solutions. Both assume a uniform grid in the x direction. Then, for the formally second order finite difference derivative on a uniform matrix, the D matrix defined in Eq.(3.1) above becomes

$$D_{2,N} = \frac{1}{2\Delta x} \begin{bmatrix} -3 & 4 & -1 & & \\ -1 & 0 & 1 & & \\ & \ddots & \ddots & \ddots & \\ & & -1 & 0 & 1 \\ & & 1 & -4 & 3 \end{bmatrix} \tag{3.18}$$

and the formally fourth order derivative matrix is given by [38],[39]

$$D_{4,N} = \frac{1}{12\Delta x}\begin{bmatrix} -25 & 48 & -36 & 16 & -3 & & & & \\ -3 & -10 & 18 & -6 & 1 & & & & \\ 1 & -8 & 0 & 8 & -1 & & & & \\ & \cdot & \cdot & \cdot & \cdot & \cdot & & & \\ & & \cdot & \cdot & \cdot & \cdot & \cdot & & \\ & & & \cdot & \cdot & \cdot & \cdot & \cdot & \\ & & & & 1 & -8 & 0 & 8 & -1 \\ & & & & -1 & 6 & -18 & 10 & 3 \\ & & & & 3 & -16 & 36 & -48 & 25 \end{bmatrix} \tag{3.19}$$

Performance of the finite difference and spectral derivatives is examined in the Results section below.

3.3 Eigenmode Calculation

After applying the boundary conditions, the discretized matrices are analyzed using eigensystem routines in the linear algebra library LAPACK[2] [40]. The routines use the QZ algorithm to calculate the eigenvalues and eigenvectors for a pair of complex, nonsymmetric matrices $\mathbf{A}$ and $\mathbf{B}$ such that $\mathbf{Ax} = \lambda\mathbf{Bx}$.

The QZ algorithm is an implementation of the commonly known QR algorithm to complex, non-Hermetian matrices. In brief, the QR algorithm operates as follows [41]:

Suppose a matrix $\mathbf{C}$ is given, and it is desired to determine its eigenvalues and eigenvectors. The Gram-Schmidt process is first used to make the columns of $\mathbf{c}$ orthonormal, which involves subtracting off the projection of the $(k+1)$th column of A from the preceding k columns, and normalizing the result. This creates an orthonormal matrix $\mathbf{Q}$ and an upper triangular matrix $\mathbf{R}$.

The QR factorization then takes the factorization of $\mathbf{C}$ into matrices $\mathbf{Q}$ and $\mathbf{R}$ and creates a new matrix $\mathbf{C}_1$ by multiplying in the opposite order:

$$\mathbf{C}_1 = \mathbf{RQ} = \mathbf{Q}^{-1}\mathbf{QRQ} = \mathbf{Q}^{-1}\mathbf{CQ} \tag{3.20}$$

This matrix has the same eigenvalues as $\mathbf{C}$, since if $\mathbf{C}_1\mathbf{x} = \mathbf{Q}^{-1}\mathbf{CQx} = \lambda\mathbf{x}$, then $\mathbf{CQx} = \lambda\mathbf{Qx}$. The eigenvalues are the same, but the eigenvectors have been scaled by $\mathbf{Q}$. A new QR factorization of $\mathbf{C}_1$ gives $\mathbf{Q}_1$ and $\mathbf{R}_1$, and then $\mathbf{C}_2 = \mathbf{R}_1\mathbf{Q}_1$ is formed. This process continues iteratively, preserving eigenvalues at every step. The sequence $\mathbf{C}_k$ approaches a diagonal or upper triangular form, and the diagonal entries approach the eigenvalues. Shifts are also employed to help convergence. Also, $\mathbf{C}$ is preprocessed into a tridiagonal form. Various other steps are taken to adapt the algorithm to the generalized eigenvalue problem, and to make it more numerically stable and efficient.

Equation (2.51) is in the form $\mathbf{Ax} = \lambda\mathbf{Bx}$. Applying the hard wall boundary condition $v_r = 0$ at the hub and the tip radius places zeros on the diagonal of matrix $\mathbf{B}$. Wu, et al. [42] suggest that one approach to avoid the mathematical difficulty associated with this matrix singularity is map the complex λ plane onto a disk via the linear transformation

$$\lambda = \frac{\tau + 1}{\tau - 1} \tag{3.21}$$

The problem then becomes the calculation of the eigenvalues τ of the system

$$-(\mathbf{A} + \mathbf{B})\mathbf{x} = \tau(\mathbf{B} - \mathbf{A})\mathbf{x} \tag{3.22}$$

The least stable mode then corresponds to the eigenvalue lying closest to the unit circle. Numerical experiments were run both using this system of equations as well as the original system (2.51), without significant differences.

3.4 Spectral eigenmode evaluation

When the eigenvalues are determined using the spectral technique described above, the resulting eigenvectors are determined at the Gauss-Lobatto points. The eigenmodes can be evaluated at points in between the Gauss-Lobatto points by employing the appropriate Chebyshev interpolation matrix.

[2]The LAPACK source distribution is available by anonymous ftp from netlib.att.com.

The interpolation matrix is based on the interpolation polynomial (3.5) at the Gauss-Lobatto points so that the value of the eigenmodes at $x \neq x_j$ (where x_j are the Gauss-Lobatto points) is given by

$$f(x) = \frac{(1-x^2)T_N'(x)}{N^2} \sum_j f(x_j) \frac{(-1)^{j+1}}{\bar{c}_j(x-x_j)} \tag{3.23}$$

3.5 ODE integration

As remarked above, calculations of the nonuniform flow eigenvalues in the literature have focussed primarily on integrating the second-order, linear, variable-coefficient ordinary differential equation for the radial behavior of the pressure. This approach was therefore examined in the present work, though ultimately not used. This section documents the reasons for doing so and the lessons learned.

For the shear flow equation (2.27) requires the solution of a two-point boundary value problem in one unknown parameter

$$\frac{d^2\bar{p}}{d\bar{r}^2} + \left(\frac{1}{\bar{r}} - \frac{2M_x'\bar{\gamma}}{\bar{\lambda}}\right)\frac{d\bar{p}}{d\bar{r}} + \left(\bar{\lambda}^2 - \frac{m^2}{\bar{r}^2} - \bar{\gamma}^2\right)\bar{p} = 0 \tag{3.24}$$

where $\bar{\lambda} = k - M_x\bar{\gamma}$, with the boundary conditions $p'(\sigma) = p'(1) = 0$.

To formulate the problem numerically, the equation was transformed to three first order equations in the variables $p_1 = p$, $p_2 = p'$, $p_3 = \bar{\gamma}$:

$$p_1' = p_2 \tag{3.25}$$

$$p_2' = -\left(\frac{1}{\bar{r}} - \frac{2M_x'p_3}{\bar{\lambda}}\right)p_2 + \left(\bar{\lambda}^2 - \frac{m^2}{\bar{r}^2} - p_3^2\right)p_1 \tag{3.26}$$

$$p_3' = 0 \tag{3.27}$$

with boundary conditions $p_2(\sigma) = p_2(1) = 0$. Note that (1) $\bar{\lambda}$ contains p_3 in it, (2) the first order system is nonlinear, and (3) the axial wavenumber has been designated the eigenvalue, since it is unknown and expected to be a constant thus satisfying $p_3' = 0$. For the swirl problem, the eigenvalue also appears in the boundary conditions.

This problem can be solved using standard boundary value techniques, such as shooting algorithms or relaxation algorithms. In the former, one boundary is fixed (say $\bar{r} = \sigma$) and the equation is integrated to the other boundary $r = 1$. In general the solution will not satisfy the boundary condition at $\bar{r} = 1$, so the error is used to correct the approximation at the first boundary and the calculation is done again. In the latter, relaxation, technique, an initial guess is made for the solution that satisfies the conditions at both boundaries but not necessarily in between. This again provides a residual error, which is used iteratively to drive the solution to convergence.

An effort was applied to implement the relaxation algorithm from [43] to solve the uniform, shear, and swirl flow ODEs. As an initial condition, the uniform flow radial acoustic modes, calculated by an alternate method, were used.

The algorithm was found to converge relatively well for the discrete set of modes analogous to the uniform flow acoustic modes. Attempts were made to map out the domains of attraction of the eigenvalues, with mixed results. One significant problem arose, however, regarding the continuum of eigenvalues. This continuum occurs when the parameter λ defined above is zero. As it approaches zero in the shear flow equation (3.24), the coefficient of $dp/d\bar{r}$ containing $1/\bar{\lambda}$ grew rapidly. The condition defining the existence of an eigenvalue is that the ODE have a nontrivial solution at those values of the parameter. In the vicinity of $\bar{\lambda} \approx 0$, the entire equation collapsed to a constant times $dp/d\bar{r}$ equals zero, which has the nontrivial solution $p(\bar{r}) = \text{constant} \neq 0$. Consequently, any time the path of integration taken by the iteration algorithm passed near $\bar{\lambda} = 0$, the iteration would stop and claim convergence.

In principle this problem can be avoided by doing an asymptotic expansion of the equation in the vicinity of $\bar{\lambda} = 0$ and proceding from there. While this was viewed as possible, the idea of applying the straightforward spectral technique described above on the original system equations proved to be far simpler, and also promised to yield the entire set of eigenvalues in one calculation rather than over several dozen runs. The results presented below are thus taken from the spectral technique, though the ODE integration was used to validate some of the sheared axial flow results.

4. Results

4.1 Validation

Validation of the discretized eigensystem analysis was performed by comparing to the analytical solutions available [44] for uniform mean axial flows and with published results for flows in lined cylindrical and annular ducts containing mean axial shear. For a uniform axial flow, the axial wavenumbers of any acoustic disturbances are given by

$$\gamma_{\text{acoustic}} = -\frac{kM_x}{1-M_x^2} \pm \frac{1}{1-M_x^2}\sqrt{k^2 + (M_x^2-1)\kappa_{m\mu}^2} \tag{4.1}$$

where $\kappa_{m\mu}$ is a separation constant for the mth circumferential and μth radial mode in the solution of the convected wave equation. The constants $\kappa_{m\mu}$ are determined using the boundary conditions. They are countably infinite and can be ordered by magnitued. The cut-off frequency is given by

$$\Delta = k^2 - (M_x^2-1)\kappa_{m\mu}^2 = 0 \rightarrow k_{\text{cut-off}} = \kappa_{m\mu}\sqrt{1-M_x^2} \tag{4.2}$$

which gives for the wavenumber

$$\gamma_{\text{cut-off}} = \frac{kM_x}{M_x^2-1} \tag{4.3}$$

When Δ is positive, the associated acoustic disturbances propagate unattenuated in the axial direction upstream and downstream from their point of origin. Otherwise the acoustic disturbances attenuate exponentially. The direction of propagation for the unattenuated waves is determined from the axial component of their group velocity,

$$v_{g,x} = \frac{dk}{d\gamma} = \pm\frac{\gamma}{\sqrt{\gamma^2+\kappa_{m\mu}^2}} + M_x\,. \tag{4.4}$$

The axial wavenumbers for any entropic and/or vortical disturbances, which are purely convected by the mean flow, are given by

$$\gamma_{\text{cv}} = \frac{k}{M_x} \tag{4.5}$$

As part of the validation of the numerical techniques, a version of the present analysis applicable to lined, two-dimensional ducts was devised. Results for a two-dimensional duct using a uniform mean flow at $M_x = -0.5$, a reduced frequency $k = -6.0$, and liners with admittance $\eta = 0.72 + 0.42i$ are shown in Table 4.1, where they are compared with those from [45]. The results taken from [45] are the results of a high-order Runge-Kutta scheme used in that paper. For the present analysis, 32 radial points were spread across the domain. Note that the two sets of results are essentially identical.

Table 4.2 uses data from the same reference, but for a duct with a uniform core flow from $y = 0$ to $y = 0.8$, and a linear Mach number profile from $y = 0.8$ to $y = 1$, where the Mach number at the boundary was set to zero. The core Mach number is $M_x = 0.3$, the reduced frequency in this case is $k = -5.0$, and the admittance is $\eta = 0.1607 + 0.4463i$. Once again, the differences are minimal.

Finally, comparison results for the flow in a lined, hollow cylinder containing a uniform flow are given in Table 4.3, where the comparison results are from [15]. This case has $m = 2$, $k = -1, M_x = 0.5$, and $\eta = 0.72 + 0.42i$. Once again, the results are in good agreement.

The data from [10] for a cylindrical duct with a shear profile

$$V_x(r) = V_0(1-r)^{1/7} \tag{4.6}$$

are shown in Table 4.4 for $M_0 = 0.3$ and $k = 20$. Table 4.5 gives results for an annulus with $\sigma = 0.85714$ and $k = 70$, with the Mach distribution

$$V_x(r) = V_0\left[1 - \frac{1}{(1-\sigma)^2}|\sigma + 1 - 2r|\right]^{1/7} \tag{4.7}$$

Table 4.1: 2D, Uniform Flow with Liner

$\gamma_n^{\pm}$	[45]	Present
γ_0^+	$1.964 - 0.003i$	$1.9636 - 0.0033i$
γ_1^+	$1.622 - 0.051i$	$1.6218 - 0.0506i$
γ_2^+	$0.979 - 0.736i$	$0.9788 - 0.7356i$
γ_3^+	$0.831 - 1.500i$	$0.8307 - 1.4999i$
γ_4^+	$0.753 - 2.219i$	$0.7531 - 2.2191i$
γ_5^+	$0.715 - 2.901i$	$0.7150 - 2.9009i$
γ_6^+	$0.691 - 3.560i$	$0.6915 - 3.5600i$
γ_7^+	$0.675 - 4.206i$	$0.6752 - 4.2060i$
γ_8^+	$0.663 - 4.844i$	$0.6633 - 4.8436i$
γ_9^+	$0.654 - 5.476i$	$0.6543 - 5.4755i$
γ_0^-	$-0.655 + 0.045i$	$-0.6547 + 0.0448i$
γ_1^-	$-0.592 + 0.074i$	$-0.5921 + 0.0740i$
γ_2^-	$-0.112 + 0.152i$	$-0.1118 + 0.1515i$
γ_3^-	$0.609 + 0.973i$	$0.6090 + 0.9733i$
γ_4^-	$0.685 + 1.820i$	$0.6851 + 1.8199i$
γ_5^-	$0.719 + 2.526i$	$0.7192 + 2.5257i$
γ_6^-	$0.744 + 3.183i$	$0.7437 + 3.1829i$
γ_7^-	$0.762 + 3.815i$	$0.7623 + 3.8154i$
γ_8^-	$0.775 + 4.433i$	$0.7752 + 4.4330i$
γ_9^-	$0.782 + 5.042i$	$0.7822 + 5.0420i$

Table 4.2: 2D, Shear Flow with Liner

$\gamma_n^{\pm}$	[45]	Present
γ_0^+	$0.6428 - 0.0215i$	$0.6431 - 0.0215i$
γ_1^+	$0.8553 - 0.0415i$	$0.8547 - 0.0410i$
γ_2^+	$-0.2853 - 0.5558i$	$-0.2852 - 0.5558i$
γ_0^-	$-1.4200 + 0.0452i$	$-1.4196 + 0.0451i$
γ_1^-	$-1.2946 + 0.0596i$	$-1.2945 + 0.0577i$
γ_2^-	$-0.3995 + 0.5634i$	$-0.3993 + 0.5633i$

The data in Table 4.6 are for a lined annulus with $M_0 = 0.3$, $k = 30$, $\sigma = 0.66667$, and $\eta = 0.3 + 0.1i$.

The lack of available results for flows with mean swirl has hampered the validation efforts in that area. An "internal consistency check" has been done, however, in the following manner. Equations (2.47), (2.48), and (2.49) can be used to express the perturbation velocity components in terms of the pressure and its radial derivative. The eigenvector $\mathbf{x}$ in the system equations (2.51) contains the computed radial distribution of all four of the perturbation variables $\bar{v}_r, \bar{v}_\theta, \bar{v}_x$, and $\bar{p}$. An internal consistency check was done by extracting the computed results for pressure from the eigenvectors corresponding to acoustic perturbations and substituting them into the analytical relations for the velocity perturbations and comparing to the remaining parts of the computed eigenvectors. In all cases examined, the comparisons gave excellent agreement. Since the computed pressure is being used, this test confirms that (1) the equations represented in the numerical code are the desired equations, and (2) high order agreement is achieved throughout the grid.

4.2 Accuracy of Numerical Discretization Technique

To test the relative accuracy of the numerical discretization techniques, a series of uniform flow cases in a hard-walled hollow cylinder was run using the parameters $M_0 = 0.181684, \sigma = 0.0$, and $k = 20.0$. This

Table 4.3: Cylinder, Uniform Flow with Liner

$\gamma_n^{\pm}$	[15]	Present
γ_0^+	$0.620 - 5.014i$	$0.6195 - 5.0139i$
γ_1^+	$-5.820 - 3.897i$	$-5.8195 - 3.8968i$
γ_2^+	$0.445 - 9.187i$	$0.4453 - 9.1868i$
γ_3^+	$0.453 - 13.062i$	$0.4539 - 13.062i$
γ_4^+	$0.480 - 16.822i$	$0.4795 - 16.822i$
γ_5^+	$0.503 - 20.531i$	$0.5029 - 20.531i$
γ_6^+	$0.522 - 24.213i$	$0.5220 - 24.213i$
γ_7^+	$0.538 - 27.880i$	$0.5376 - 27.880i$
γ_8^+	$0.550 - 31.537i$	$0.5502 - 31.537i$
γ_9^+	$0.589 - 49.75i$	$0.5891 - 49.754i$
γ_0^-	$0.410 + 1.290i$	$0.4101 + 1.2904i$
γ_1^-	$1.259 + 6.085i$	$1.2595 + 6.0852i$
γ_2^-	$1.146 + 9.668i$	$1.1457 + 9.6679i$
γ_3^-	$1.022 + 13.315i$	$1.0218 + 13.315i$
γ_4^-	$0.943 + 16.977i$	$0.9425 + 16.977i$
γ_5^-	$0.891 + 20.635i$	$0.8908 + 20.635i$
γ_6^-	$0.855 + 24.288i$	$0.8549 + 24.288i$
γ_7^-	$0.829 + 27.937i$	$0.8288 + 27.937i$
γ_8^-	$0.809 + 31.581i$	$0.8089 + 31.581i$
γ_9^-	$0.755 + 49.77i$	$0.7547 + 49.772i$

Table 4.4: Cylinder, Shear Flow

$\gamma_n^{\pm}$	Shankar [10]	16 points	32 points
γ_0^-	0.81500	0.81600	0.81547
γ_1^-	0.76944	0.76956	0.76952
γ_2^-	0.72751	0.72766	0.72763
γ_3^-	0.65329	0.65342	0.65346
γ_4^-	0.54028	0.54035	0.54051
γ_5^-	0.36933	0.36937	0.36975
γ_6^-	0.06361	0.06491	0.06477
γ_7^-	$-0.28313 + 0.48807i$	$-0.27836 + 0.48717i$	$-0.28277 + 0.48650i$
γ_8^-	$-0.28357 + 0.80635i$	$-0.28775 + 0.86216i$	$-0.28328 + 0.80439i$
γ_9^-	$-0.28410 + 1.05658i$	$-0.26178 + 1.0964i$	$-0.28368 + 1.0539i$
γ_{10}^-	$-0.28410 + 1.27947i$	$-0.38211 + 1.6308i$	$-0.28403 + 1.2756i$

corresponded to the case examined in Table 1 of [46]. The output parameter of interest in [46] was $K = \gamma/k$, which was computed from the second-order differential equation for pressure using a 4th-order accurate Runge-Kutta method.

Figures 4.1, 4.2, 4.3, and 4.4 plot the natural log of the error against the natural log of the number of radial points, for the eigenvalue corresponding to the 0th, 1st, 2nd, and 3rd acoustic modes.

The finite difference approximations use an equally-spaced grid and the derivative matrices given in (3.18) and (3.19). The spectral discretization uses the Chebyshev-Gauss-Lobatto points and the derivative matrix in (3.7). Each figure also shows a dotted line representing formal second and fourth order accuracy.

In general, the second and fourth order finite difference approximations follow the formal definitions. The spectral accuracy is significantly greater for all numbers of grid points, and is the scheme utilized in the presentation of further results below.

Table 4.5: Annulus, Shear Flow

$\gamma_n^{\pm}$	Shankar [10]	Present
γ_0^-	0.79293	0.79353
γ_1^-	0.75075	0.75292
γ_2^-	0.57143	0.57320
γ_3^-	-0.00969	0.16437
γ_4^-	$-0.28733 + 0.73219i$	$-0.28357 + 0.73425i$
γ_5^-	$-0.29118 + 1.21721i$	$-0.28622 + 1.2198i$
γ_6^-	$-0.29248 + 1.62569i$	$-0.28766 + 1.6281i$
γ_7^-	$-0.29519 + 2.00221i$	$-0.28947 + 2.0055i$
γ_8^-	$-0.29567 + 2.36511i$	$-0.29035 + 2.3683i$
γ_9^-	$-0.29768 + 2.71665i$	$-0.29167 + 2.7209i$
γ_{10}^-	$-0.29776 + 3.06414i$	$-0.29243 + 3.0679i$

Table 4.6: Lined Annulus, Shear Flow

$\gamma_n^{\pm}$	Shankar [10]	Present
γ_0^-	$0.78698 + 0.00400i$	$0.78093 + 0.00913i$
γ_1^-	$0.73438 + 0.02541i$	$0.75079 + 0.03387i$
γ_2^-	$0.55840 + 0.03148i$	$0.57267 + 0.03246i$
γ_3^-	$0.14308 + 0.07638i$	$0.16875 + 0.06982i$
γ_4^-	$-0.23900 + 0.74173i$	$-0.23734 + 0.72727i$
γ_5^-	$-0.26149 + 1.21973i$	$-0.25993 + 1.2120i$
γ_6^-	$-0.26996 + 1.62627i$	$-0.26860 + 1.6207i$
γ_7^-	$-0.27669 + 2.00192i$	$-0.27468 + 1.9983i$
γ_8^-	$-0.27974 + 2.36439i$	$-0.27813 + 2.3612i$
γ_9^-	$-0.28359 + 2.71568i$	$-0.28147 + 2.7139i$
γ_{10}^-	$-0.28502 + 3.06304i$	$-0.28361 + 3.0610i$

4.3 Swirling Flows

The remaining results illustrate the effect of swirl on the axial wavenumbers and radial modes of any unsteady disturbances. The baseline case is taken to be a mode with two nodal diameters, $m = 2$, with axial Mach number $M_x = 0.3$, reduced frequency $k = 10.0$, and hub-to-tip ratio $\sigma = 0.25$. Swirl is provided by specifying the amplitude of a free vortex, i.e.,

$$V_\theta(r) = \frac{\Gamma}{r}. \tag{4.8}$$

Figure 4.5 shows the real vs the imaginary parts of the axial wavenumbers for the baseline case with no swirl. The figure shows the classical result, in that the line to the left of the imaginary axis represents the analytic cut-off condition, two families of propagating acoustic modes are distributed symmetrically about the cut-off wavenumber, and a doubly-infinite set of attenuated modes exist with real parts equal to the cut-off wavenumber, $\mathrm{Re}\{\gamma_{\mathrm{cut-off}}\} = -1.5707$. Eigenvalues that are purely real indicate unattenuated propagation, while for the complex eigenvalues the imaginary part gives the growth or decay rate, c.f. (2.23) and (4.1). Physical arguments are used to eliminate growing acoustic modes in either direction. In addition, the eigenvalues corresponding to the convected disturbances all fall on top of one another at the convected wavenumber $\gamma_{\mathrm{cv}} = 33.3$.

Free vortex swirl with magnitude $\Gamma = 0.2$ is then added to the mean flow, giving the Mach number distribution shown in Figure 4.6. The axial wavenumbers from both the uniform flow case and the swirling flow case are shown in Figure 4.7. The effect of the swirl on the discrete sets of modes corresponding to the

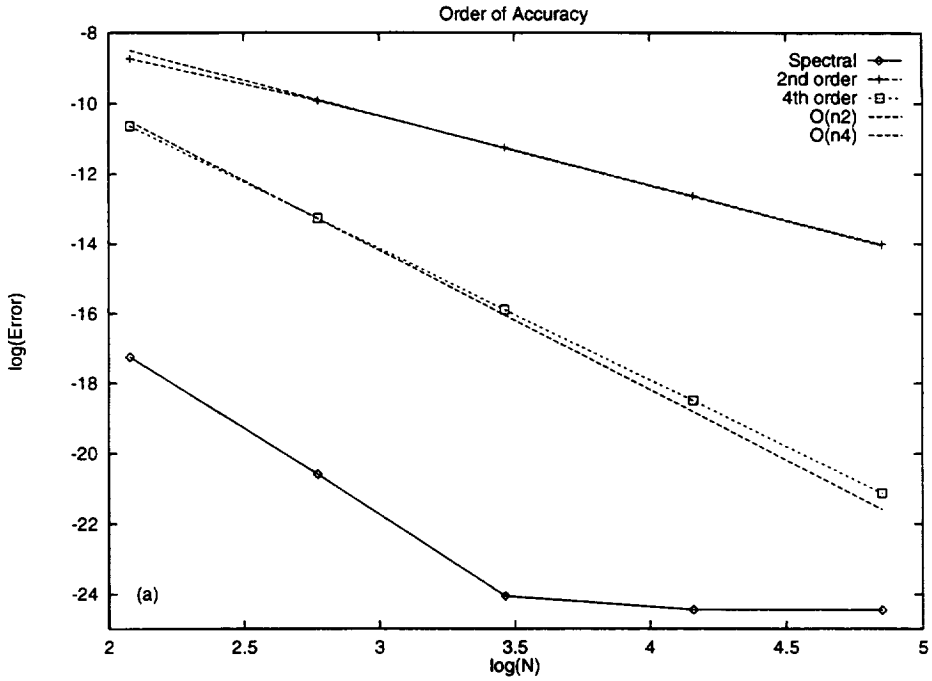

Figure 4.1: Order of accuracy for mode 0.

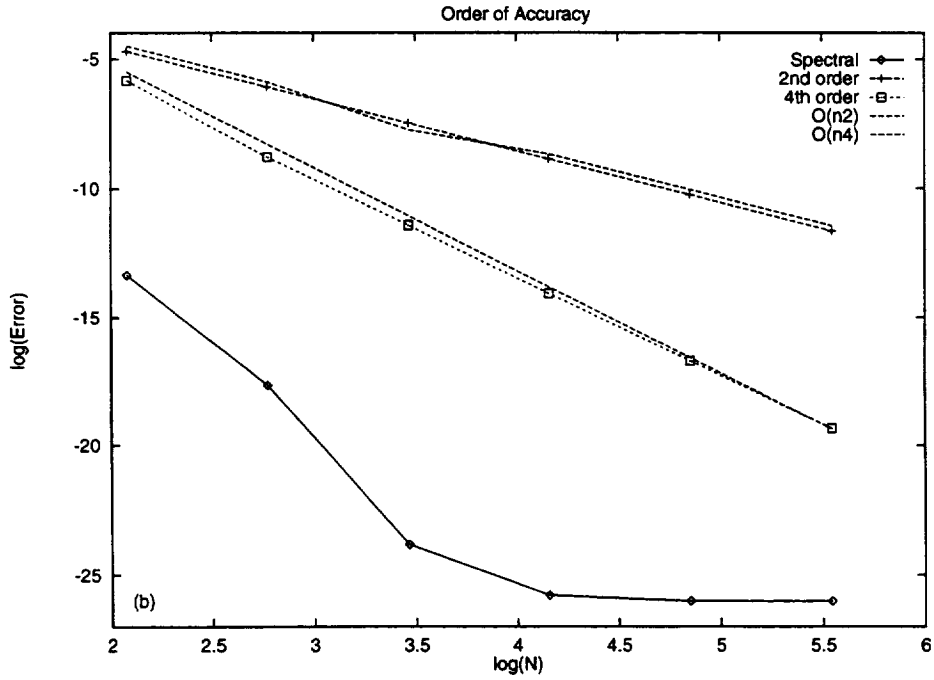

Figure 4.2: Order of accuracy for mode 1.

acoustic modes in uniform mean flow is largest near cut off and tends to vanish for large mode order. One pair of the uniform flow acoustic modes has become cut off with swirl present. The isolated uniform flow convected mode, however, has split into a set of points covering the continuum range from $\gamma_{cv,min} = k/M_x(1) = 12.0$ to $\gamma_{cv,max} = k/M_x(\sigma) = 32.0$, since the nonuniform mean flow implies different velocities at different grid points. Adding additional grid points to the calculation merely covers the continuum more densely without

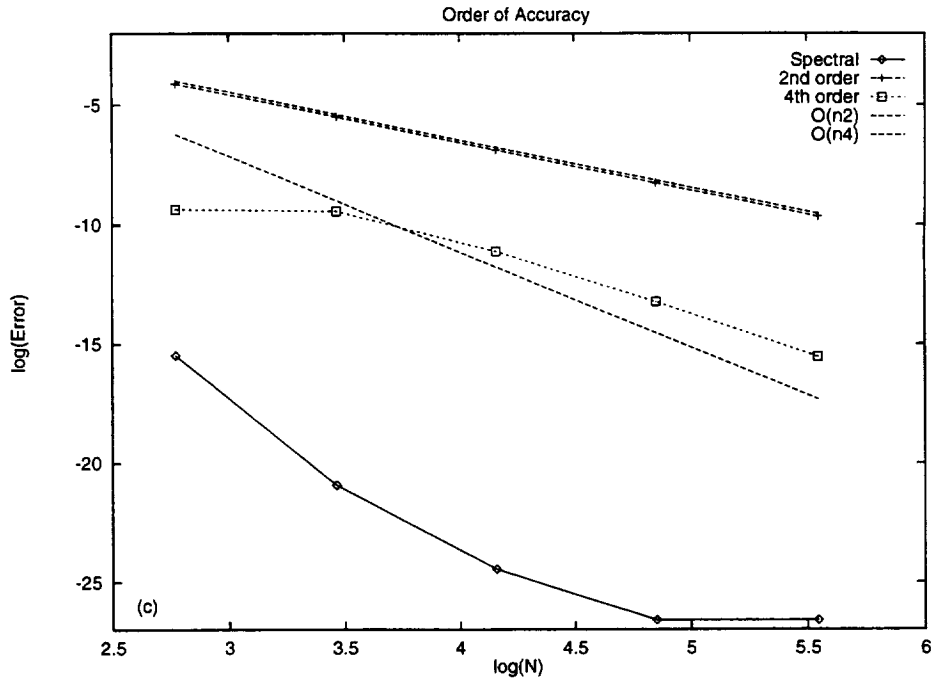

Figure 4.3: Order of accuracy for mode 2.

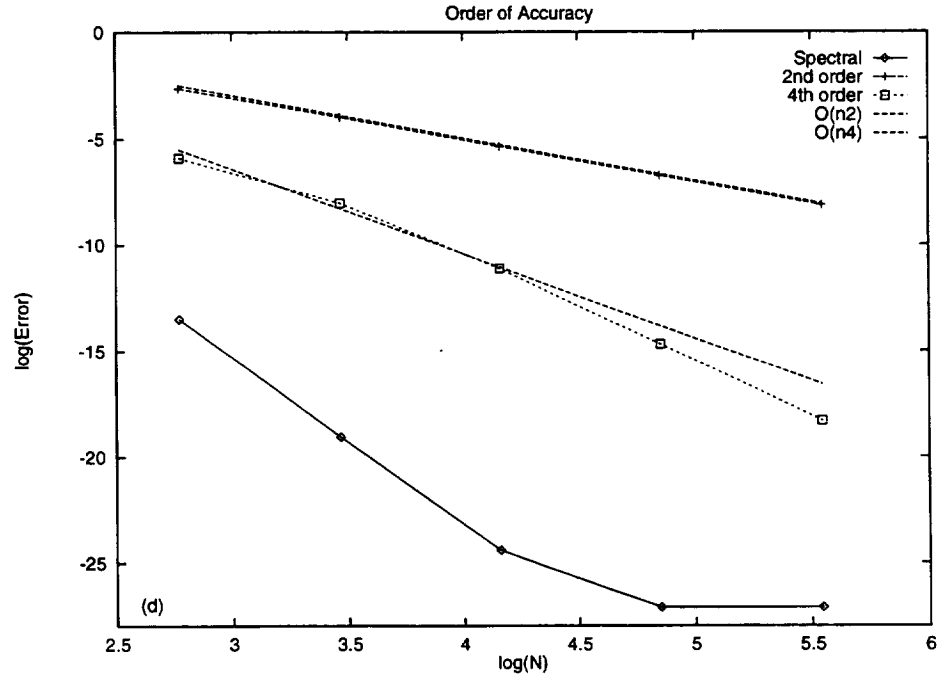

Figure 4.4: Order of accuracy for mode 3.

changing its minimum or maximum values.

Figures 4.8 and 4.9 illustrate the real and imaginary distributions of pressure for the $\kappa_{2,0}$ and $\kappa_{2,2}$ modes, respectively. The radial acoustic modes are indexed by the number of times their real parts cross zero. It is interesting to observe that the unattenuated mode $\kappa_{2,0}$ is almost purely real, while the exponentially decaying mode $\kappa_{2,2}$ is complex.

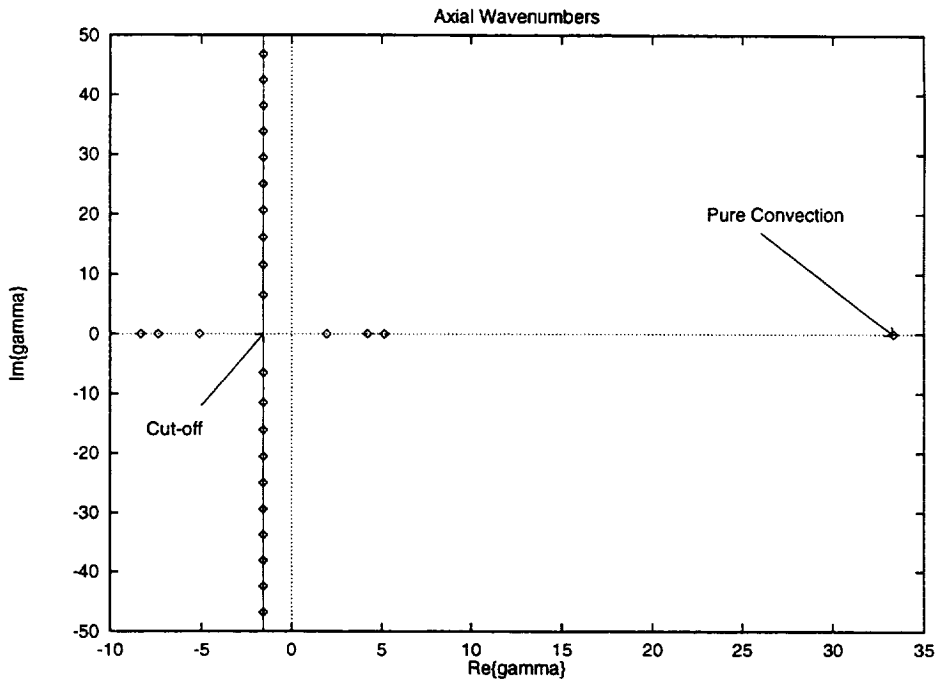

Figure 4.5: Uniform mean flow wavenumbers. The discrete set symmetric about the cut-off line correspond to acoustic modes propagating upstream and downstream, while modes on the cut-off line are attenuated as they move axially. The point labelled "pure convection" is the repeated wave number for all the convected modes.

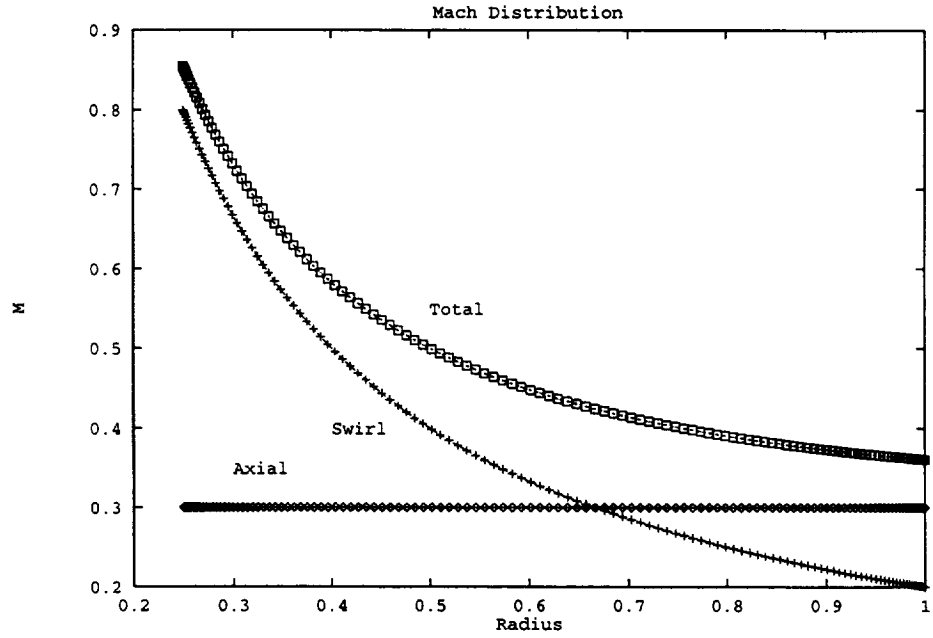

Figure 4.6: Mach distribution for swirl case.

The eigensystem analysis computes the complete eigenvector given by $\mathbf{x} = \{\bar{v}_r, \bar{v}_\theta, \bar{v}_x, \bar{p}\}$, and thus computes the radial distributions of the radial, circumferential, and axial velocities along with the pressure.

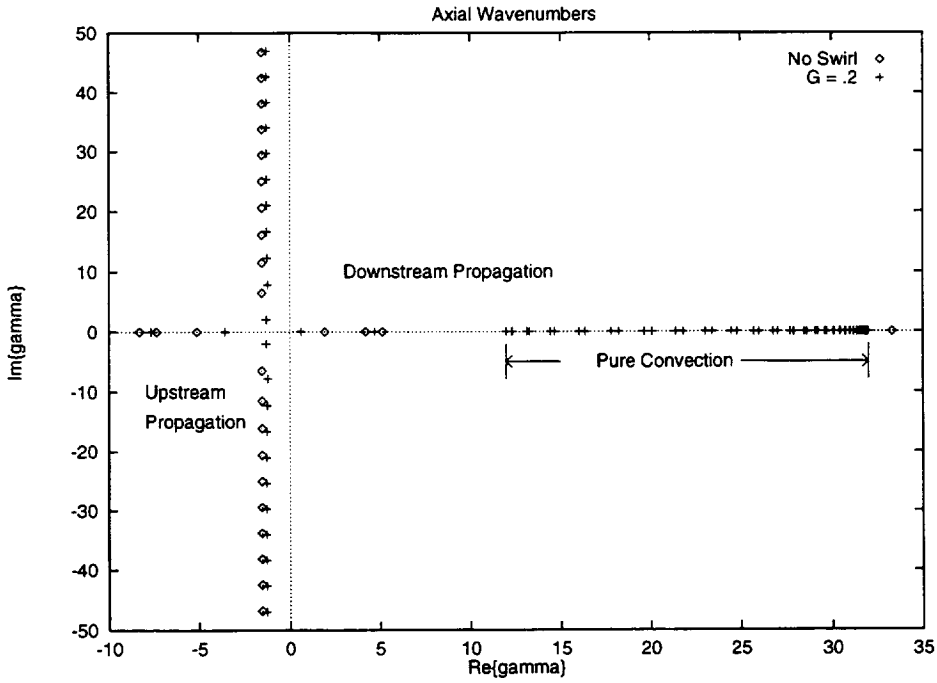

Figure 4.7: Effect of free vortex swirl.

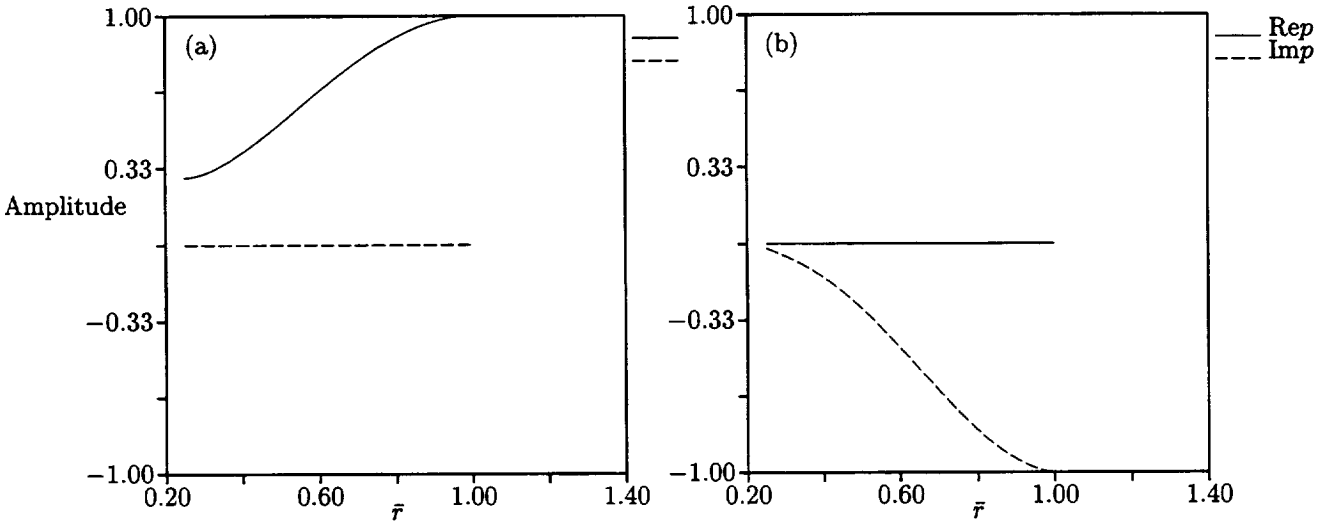

Figure 4.8: Cut on pressure mode $\kappa_{2,0}$ for (a) uniform flow and (b) free vortex swirl with $\Gamma = 0.2$.

Simple algebra can be applied to (2.51) to express the velocity components in terms of pressure and its radial derivative, and this provides a convenient check of the consistency of the algorithm. Figures 4.10 and show the real and imaginary parts of all the disturbance quantities for modes $\kappa_{2,0}$ and $\kappa_{2,2}$, respectively, both with and without swirl. For the uniform axial flow cases, the velocity modes do correspond to the analytic formulas applied to the acoustic part of the overall eigenmode. The qualitative effect of adding the swirl can be seen in Figure 4.11. Note in particular that the slope $d\bar{p}/d\bar{r}$ of the acoustic eigenmodes at the hub and tip boundaries is not zero in the swirl cases as it is in uniform flow. This situation is particularly evident at the hub, where the swirl Mach number is greatest.

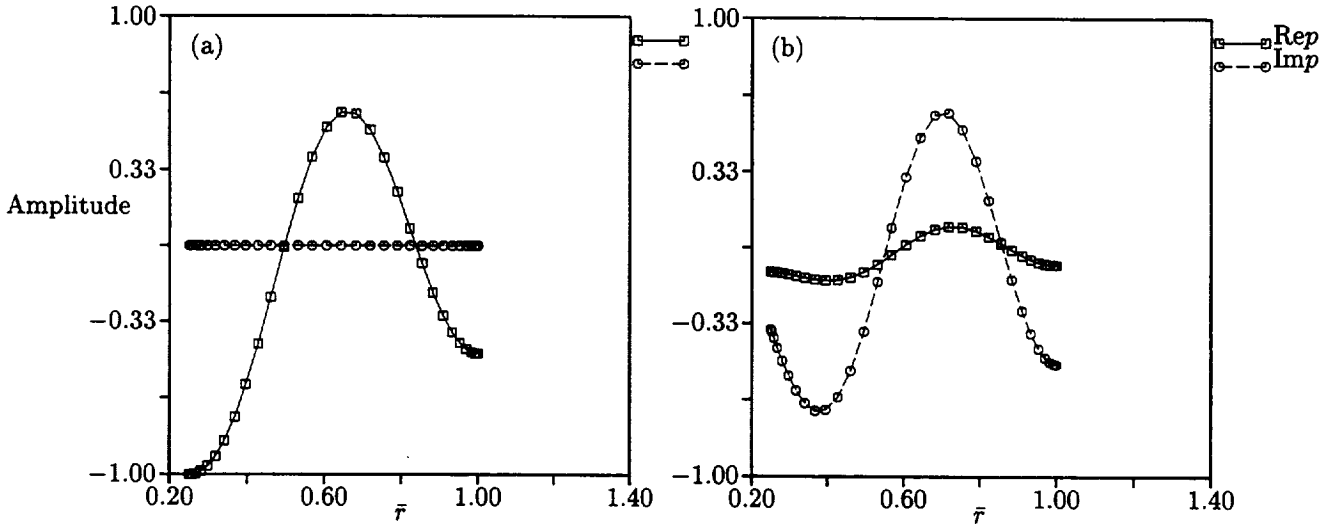

Figure 4.9: Cut off pressure mode $\kappa_{2,2}$ for (a) uniform flow and (b) free vortex swirl with $\Gamma = 0.2$.

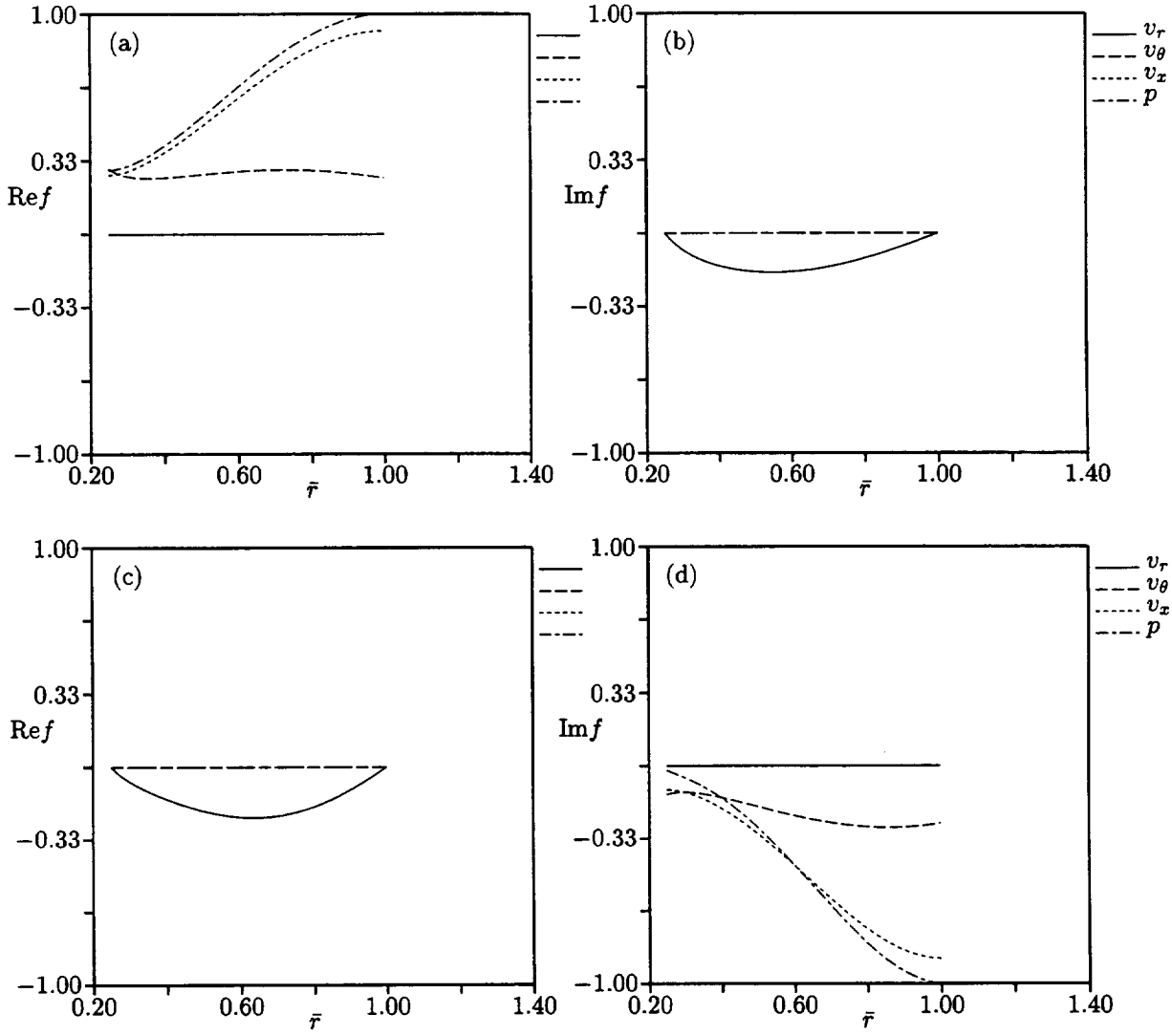

Figure 4.10: Real and imaginary parts of the radial distributions of $f(\bar{r})$ where $f = \bar{v}_r, \bar{v}_\theta, \bar{v}_x$, and $\bar{p}$ for mode $\kappa_{2,0}$. (a) and (b): uniform flow; (c) and (d): $\Gamma = 0.2$.

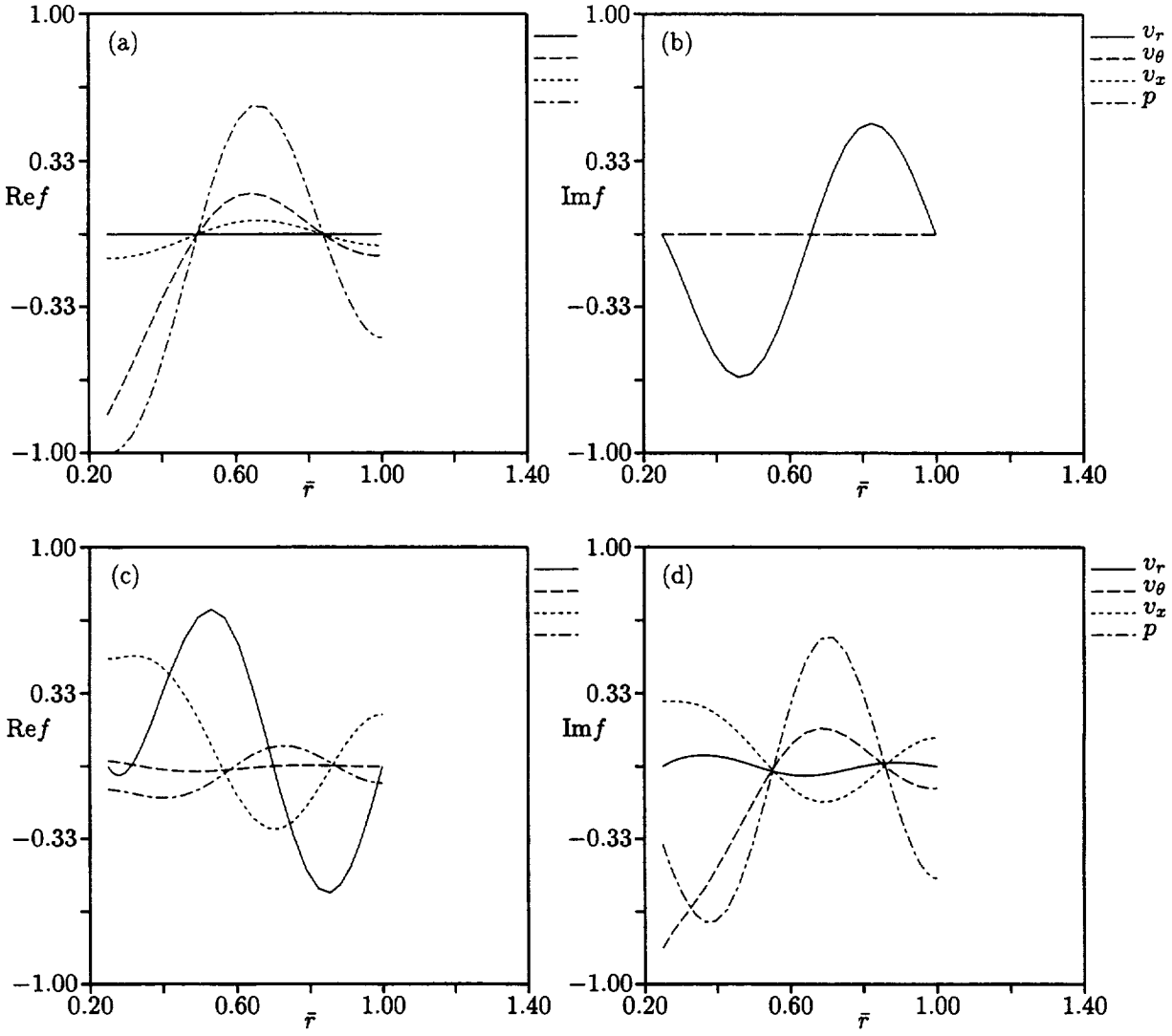

Figure 4.11: Real and imaginary parts of the radial distributions of $f(\bar{r})$ where $f = \bar{v}_r, \bar{v}_\theta, \bar{v}_x$ and $\bar{p}$ for mode $\kappa_{2,2}$. (a) and (b): uniform flow; (c) and (d): $\Gamma = 0.2$.

5. Unresolved Issues

This section documents issues that have not yet been resolved in the present analysis.

5.1 Hydrodynamic stability

A necessary but not sufficient condition for instability for axisymmetric (i.e., $m = 0$) disturbances in the inviscid limit is the vanishing of $\frac{d}{dr}\left(\frac{1}{r}\frac{dV_x}{dr}\right)$ somewhere in the flow[1]. This condition is analogous to the existence of an inflection point in a two-dimensional shear flow profile. Also, if an instability is to exist (also for $m = 0$) then the phase velocity of the disturbance $v_\phi = k/\bar{\gamma}$ must be equal to the mean flow velocity at some point in the flow.

In an inviscid fluid in a cylindrical or annular duct, Kelvin's theorem states that the circulation along any ring at radius r will be a constant. For a swirling mean flow, the circulation is given by $\Gamma = 2\pi r V_\theta =$ constant. The following stability argument is due to Von Karman [49]. Define the quantity

$$k(r) = rV_\theta(r) \tag{5.1}$$

then the centripetal acceleration at any radius is given by $V_\theta^2/r = k^2/r^3$. Consider a ring at radius r_1, having velocity $V_{\theta,1} = V_\theta(r_1)$ and $k_1 = r_1 V_{\theta,1}$, and displace a fluid particle in this ring to a radius $r_2 > r_1$.

The centripetal force on the displaced particle is then given by

$$f_{\text{centrip}} = \rho\frac{k_1^2}{r_2^3} \tag{5.2}$$

while the pressure gradient at r_2 is

$$f_{\text{pressure}} = \rho\frac{k_2^2}{r_2^3} \tag{5.3}$$

so the fluid is stable (i.e., the restoring pressure force is greater than the displacing centripetal force) if

$$\frac{k_1^2}{r_2^3} < \frac{k_2^2}{r_2^3} \tag{5.4}$$

implying that $k^2(r)$ increases outward.

For a solid body swirl, $V_\theta = \Omega r$ so $k = \Omega r^2$. This increases outward for all r, and is thus stable. For a free vortex swirl, $V_\theta = \Gamma/r$ so $k = \Gamma$. This is a constant, which would seem to imply neutral stability. In order to have a test case that would give instability, a swirl flow of the form $V_\theta = \beta/r^2$ was implemented. This gives $k = \beta/r$, which decreases outward.

In order to examine the stability of unsteady perturbations in the flow, a test due to Briggs [50] (and used in Tam and Hu [51] and Hu [52]) is used. It involves deformations of contours in the complex plane as part of an inversion of a Laplace transform. Letting ω be complex, the eigenvalue problem is solved for a series of frequencies $\omega = \omega_R + i\omega_I$, where ω_R is the desired frequency and ω_I is steadily reduced to zero. Any zeros originating in the upper half of the γ plane are downstream propagating waves, and zeros from the lower half of the γ plane are upstream propagating waves. Any zeros that move across the real γ axis are instability waves. All the others either propagate unattenuated (neutrally stable) or decay exponentially.

Figures 5.1 and 5.2 illustrate this process applied to the special swirl cases $V_\theta = \Gamma/r$ and $V_\theta = \beta/r^2$. The axial flow was uniform at $M_x = 0.2$, along with $\sigma = 0.5, \beta = 0.2$, and $m = 2$. For both figures, the discrete eigenvalues move from their values for $k = 10 + 2i$ to their values at $k = 10$ smoothly, without crossing the real axis. The range of convected modes between $\text{Re}\{\gamma\} = 32$ to $\text{Re}\{\gamma\} = 48$ for the free vortex swirl case also do not cross the real axis.

In the contrived case $V_\theta = \beta/r^2$, however, the convected modes have split into an oval pattern, which (when k is purely real) is symmetric about the real axis. Consequently, when k is given a finite imaginary part, part of the oval crosses the real axis indicating instabilities.

The oval nature of the convected roots has not been verified by previous investigations. A grid resolution study appears in Figure 5.3 (note the expanded ordinate scale). While the discrete roots have clearly converged, the oval structure is still shrinking toward the real axis as more and more points are added. While it is possible that this behavior is an illustration of so-called pseudo-eigenvalues[2] and therefore physically

[1] This condition, attributed to Rayleigh, is discussed in [47] and [48].

[2] If eigenvalues are defined as λ such that $||\mathbf{A} - \lambda\mathbf{I}|| = 0$, then the pseudo-eigenvalue λ_ϵ satisfies $||\mathbf{A} - \lambda_\epsilon\mathbf{I}|| \leq \epsilon$.

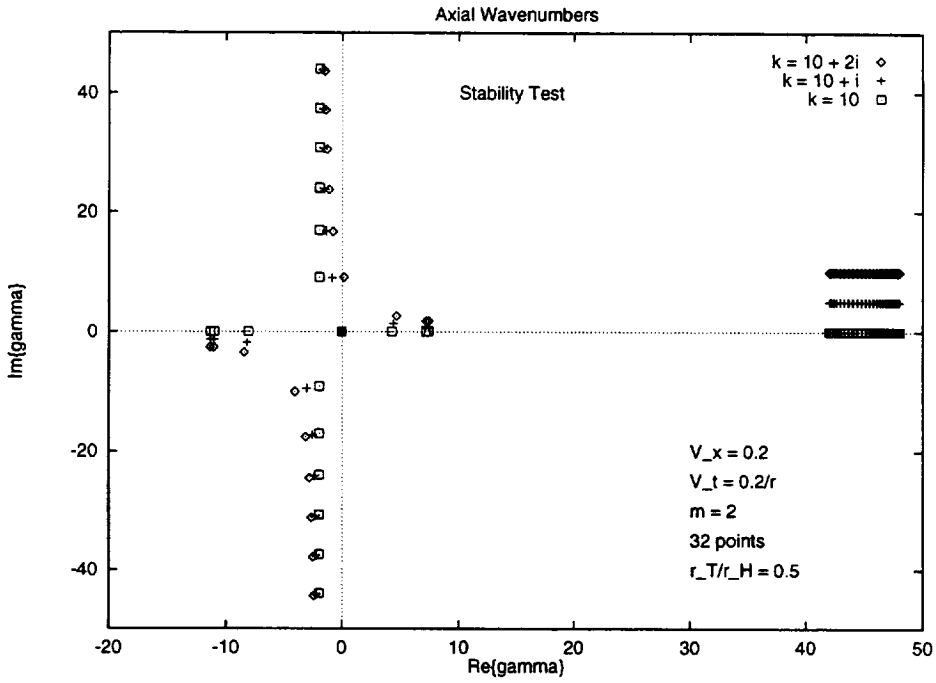

Figure 5.1: Stability of free vortex swirl.

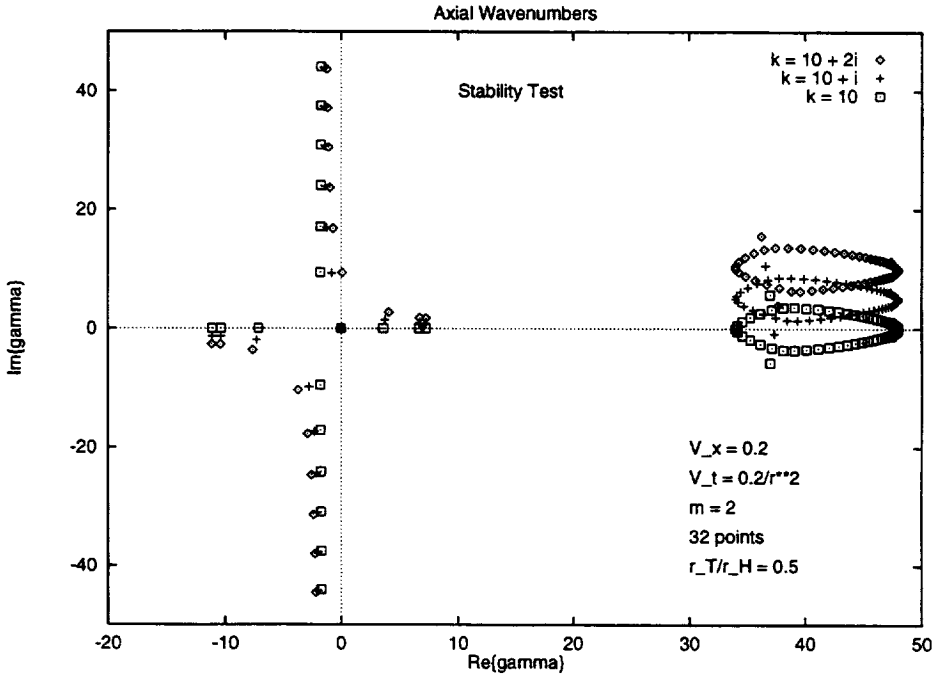

Figure 5.2: Stability of $V_\theta = \beta/r^2$.

real, further checks are required.

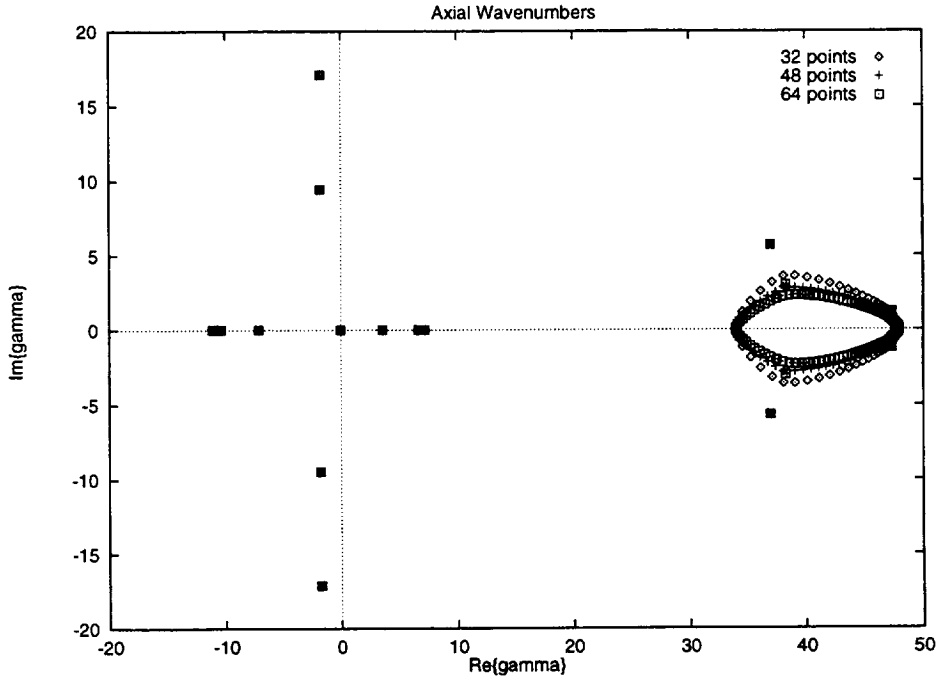

Figure 5.3: Grid independence study for oval structure.

5.2 Completeness

The form of the unsteady perturbations assumed in (2.23) is equivalent to taking Fourier transforms in the axial and circumferential directions and in time. While considerable evidence in favor of this assumption exists for the independent variables θ and t, the situation is not as clear in the x direction. In fact, recent work by Goldstein and Wundrow [25] suggests that the vortical part of the unsteady velocity in a swirling potential flow (i.e., free vortex) has an algebraic dependence on x. Tan[53, 54, 55], however, has suggested that the dependence is linear in x near the source of the disturbance but proportional to $1/x$ later. Resolution of this issue is critical for completeness, since if the modes have an algebraic dependence on x, the axial behavior is neither bounded nor square integrable so the exponential assumption for the axial behavior is not valid.

It is interesting to note that the exponential assumption arises naturally from a separation of variables type analysis. The matrix equations are given by (2.51). If the form for the unsteady perturbations is generalized to

$$\tilde{v}_r(r,\theta,x,t) = v_r(r)X(x)e^{i(m\theta-\omega t)} \tag{5.5}$$

$$\tilde{v}_\theta(r,\theta,x,t) = v_\theta(r)X(x)e^{i(m\theta-\omega t)} \tag{5.6}$$

$$\tilde{v}_x(r,\theta,x,t) = v_x(r)X(x)e^{i(m\theta-\omega t)} \tag{5.7}$$

$$\tilde{p}(r,\theta,x,t) = p(r)X(x)e^{i(m\theta-\omega t)} \tag{5.8}$$

then a matrix differential equation can be written for the axial behavior, $X(x)$,

$$\mathbf{Au} = -\frac{\mathbf{X}'}{\mathbf{X}}\mathbf{Bu} \tag{5.9}$$

where

$$\mathbf{A} = \begin{bmatrix} V_x & 0 & 0 & 0 \\ 0 & V_x & 0 & 0 \\ 0 & 0 & V_x & 1 \\ 0 & 0 & 1 & V_x \end{bmatrix} \tag{5.10}$$

and

$$\mathbf{B} = \begin{bmatrix} i\left(\frac{m}{r}V_\theta - \omega\right) & -\frac{2V_\theta}{r} & 0 & \frac{1}{\bar{\rho}}\left(D - \frac{V_\theta^2}{rA^2}\right) \\ \frac{V_\theta}{r} + \frac{dV_\theta}{dr} & i\left(\frac{m}{r}V_\theta - \omega\right) & 0 & \frac{im}{\bar{\rho}r} \\ \frac{dV_x}{dr} & 0 & i\left(\frac{m}{r}V_\theta - \omega\right) & 0 \\ \frac{V_\theta^2}{rA^2} + \frac{1}{r} + D & \frac{im}{r} & i\left(\frac{m}{r}V_\theta - \omega\right) & \end{bmatrix} \tag{5.11}$$

and $\mathbf{u} = \{v_r, v_\theta, v_x, p\}^T$. This reduces to the form given in (2.51) when $-X'/X = \lambda =$ constant. If (5.9) is viewed as an ordinary differential equation in x, then it can be solved in terms of matrix exponentials as

$$\mathbf{X}(x) = \mathbf{X}_0 e^{-\mathbf{B}^{-1}\mathbf{A}x} \tag{5.12}$$

This process fails if $\mathbf{B}$ is singular, which will occur at no-slip boundaries where $M_x = 0$.

It should be noted that if the axial wavenumbers in Eqn.(2.23) are assumed *a priori* to have a radial dependence, i.e.,

$$\tilde{v}_r(r, x) = v_r(r)e^{i\gamma(r)x} \tag{5.13}$$

and likewise for the other unsteady variables, then the radial derivatives appearing in (2.51) produce an additional term:

$$\frac{\partial \tilde{v}_r}{\partial r} = \left(\frac{dv_r}{dr} + i\frac{d\gamma}{dr}x\right)e^{i\gamma x} \tag{5.14}$$

This does introduce an algebraic dependence on x, and must be examined further.

An alternative approach, which takes advantage of the existing theorems on completeness, is to use the symmetric form of the nonlinear Euler equations [56]. Subsequent linearization will maintain the symmetric form, and the theory states that any normal operator can be both diagonalized and symmetrized, thus giving a complete set of eigenvalues. This approach has not yet been pursued, but appears to be viable.

6. Conclusions

The eigenvalues and eigenvectors for nonuniform mean flows in annular and cylindrical ducts have been calculated using a discretized form of the first order linearized Euler equations. Three numerical discretization techniques have been applied to the first order system; a Chebyshev collocation technique, second-order finite differences, and fourth-order finite differences. The resulting complex, nonhermetian, generalized eigenvalue problems were solved using the QR algorithm from LAPACK. The analysis has been validated for uniform flows and for shear flows with and without acoustic liners. Results have also been presented for annular ducts containing free vortex swirl.

The axial wavenumbers of the nonuniform mean flows are seen to fall into two distinct classes: a discrete set corresponding to the acoustic modes in uniform mean flows, and a continuous set along the local convected speeds of the mean flow.

Although the code has been validated for lined annular and cylindrical ducts containing axial shear flows, the lack of published results for swirling flows has hampered efforts in this area. Instead, the internal consistency of the code has been verified. The spectral discretization technique has been compared to the finite difference approximations and found to be significantly more accurate for a given number of radial grid points.

Questions still remain regarding the completeness of the calculated eigensystem, particularly in reference to any algebraic dependence in the axial direction of the unsteady disturbances. Efforts to resolve this issue will be made, partly through the use of assumed radial dependence of the axial wavenumbers. In addition, the stability test advocated by Briggs has been used to examine ostensibly unstable flows, but, other than the appearance of an oval shaped region around the convected wavenumbers, no instabilities have been detected. Work must also be done to determine whether the oval region itself is an indication of physical pseudo-eigenvalues in the system or simply a sensitive detector of subtle errors in the analysis.

7. Acknowledgements

The author would like to acknowledge the considerable contributions and help received from Professor David Gottlieb and his students at Brown University. In addition, the author would like to thank Dr. Marvin Goldstein and Dr. David Wundrow of NASA Lewis Research Center for their assistance, and Dr. Choon Tan of MIT for his help. The author would also like to thank Dr. Donald Hanson and Mr. David Topol of Pratt & Whitney Aircraft and Dr. Harold Meyer of Hamilton Standard, and Dr. Joseph Verdon of United Technologies Research Center for many fruitful discussions during this project.

8. Appendix: The *Swirl* Code

The algorithms described above for analyzing axial flows with mean shear and swirl in lined and unlined ducts have been implemented into a code named SWIRL.

The code is written in Fortran 77 with some relatively standard extensions, all of which eventually became part of the Fortran 90 standard. Double precision complex data types were used to try to achieve the maximum possible numerical accuracy. To facilitate interaction with the user, the "NAMELIST" has been employed, in a form compatible with the Fortran 90 standard. It should be noted, however, that the specific format of NAMELIST interaction statements varies from system to system. For example, on the IBM RS6000 workstation where the code was developed, the user types " &inputs omega = 10.0 &end" to communicate with the program.

To faciliate both portability and reliability of the program, standard freely-available numerical libraries were used wherever possible in the algorithm. These include the numerical linear algebra library LAPACK (which also makes use of the Basic Linear Algebra Subroutine, or BLAS, library), and the basic curve fitting routines contained within the FITPACK library. Rather than expect the user to download and install these libraries, the revelent routines were extracted from them and are included in different subdirectories of the SWIRL code distribution.

8.1 Input Quantities

A sample input file, *input.data*, is included in the distribution. The sample file is reproduced here for reference:

```
&inputs
 mm    = 2, npts  =    32,  sig   = 0.50, akre  =  10.,  akim = 0.,
 ir    = 1, rmax  =  0.30,  slope = 0.00,
 is    = 1, angom =  0.50,  gam   = 0.00, irepeat = 0, ifd = 0,
 itest = 0, etahr =  0.00,  etahi = 0.00, etadr = 0.00, etadi = 0.00,
 ed2   = 0.0, ed4 = 0.0
&end
```

where the various quantities are described in Table 8.1. The sample file thus represents a search for the axial wavenumbers for 2-lobed modes of frequency $\omega = 10$ in a hard-walled duct with radius ratio 0.5, containing a uniform axial mean flow at mach number $M_z = 0.3$ and a solid body swirl flow with $\Omega = 0.5$. Thirty-two points are distributed on a Gauss-Lobatto grid across the duct, implying that the resulting wavenumbers associated with modes with up to 9 zero crossings are expected to be reproducable.

The code itself contains a significant number of comments intended as documentation. Of particular interest are the subroutines determining the form of the mean flow in the duct, namely, *rmach.f*, *smach.f*, and *sndspd.f*. The first, *rmach.f*, contains options for choosing the form of the axial shear flow. The second, *smach.f*, describes options for the mean swirl distribution, and the last, *sndspd.f*, determines the radial dependence of the mean speed of sound. Note that a specified distribution can in principle be entered for all three, but that the resulting speed of sound distribution is not likely to satisfy the isentropic conditions assumed in the analysis unless this was taken into account ahead of time.

8.2 Output Files and Testing

Two test output files are included in the distribution: *gammas.test* and *gam.non.test*. The former contains the real and imaginary parts of all the axial wavenumbers calculated by the code. The latter contains only those wavenumbers associated with the nonconvected modes (generally acoustic), sorted by number of zero crossings in the mode. The code generates the analogous files *gammas.dat* and *gam.nonconv*, which should be compared to the above, and the file *cv.waves.dat* which holds the data for the convected waves. The wavenumber comparison is most easily carried out using a plotting package like the freely-available program GNUPLOT. To facilitate comparisons using this program, any lines in the output files containing nonnumeric data begin with an initial "#".

Table 8.1: Description of Input Quantities

mm	Circumferential mode number
npts	Number of radial mesh points
sig	Hub-to-duct radius ratio, σ
akre	Real part of frequency, $k = \omega r_D / A_T$
akim	Imag part of frequency (zero except for stability calcs)
ir	Axial Mach distribution number (for details see *rmach.f*) 0 = Uniform 1 = Linear shear 2 = Read from file 3 = Uniform + sine wave bndry layers of thickness δ 4 = Uniform + linear bndry layers 5 = Uniform + 1/7th power law bndry layers 6 = Hyperbolic secant profile 7 = Laminar mean flow 8 = Wavy sinusoid (for stability calcs) 9 = Hagen-Poiseuille flow
rmax	Maximum axial Mach number
slope	slope of linear Mach distribution; also used as boundary layer thickness
is	Swirl Mach distribution number (for details see *smach.f*) 0 = No swirl 1 = Solid body swirl 2 = Free vortex swirl 3 = Solid body and free vortex together 4 = $V_\theta = 1/r^2$ (for stability calcs) 5 = Read from file 6 = Constant swirl across the duct 7 = Trailing line vortex
angom	Magnitude of solid body swirl $V_\theta = \Omega r$; also used as constant for constant swirl
gam	Magnitude of free vortex swirl $V_\theta = \Gamma / r$
ifd	Use finite differences for derivatives 1 = Second order 2 = Fourth order
itest	Perform consistency test on selected modes
etahr	Real part of hub liner admittance
etahi	Imag part of hub liner admittance
etadr	Real part of duct liner admittance
etadi	Imag part of duct liner admittance
ed2	Second order smoothing for derivatives
ed4	Fourth order smoothing for derivatives

Bibliography

[1] Verdon, J. M., "The Unsteady Flow in the Far Field of an Isolated Blade Row," *Journal of Fluids and Structures*, Vol. 3, No. 2, March 1989, pp. 123–149.

[2] Tyler, J. M. and Sofrin, T. G., "Axial Flow Compressor Noise Studies," *SAE Transactions*, Vol. 70, 1962, pp. 309–332.

[3] Hanson, D. B., "Mode Trapping in Coupled 2D Cascades–Acoustic and Aerodynamic Results," Paper 93-4417, AIAA 15th Aeroacoustics Conference, Long Beach, CA, October 1993.

[4] Meyer, H. D., "Effect of Inlet Reflections on Fan Noise Radiation," Paper 93-4427, AIAA 15th Aeroacoustics Conference, Long Beach, CA, October 1993.

[5] Hanson, D. B., "Coupled 2-Dimensional Cascade Theory for Noise and Unsteady Aerodynamics of Blade Row Interaction in Turbofans, Volume 1–Theory Development and Parametric Studies," CR 4506, NASA, 1994.

[6] Giles, M. B., "Non-reflecting Boundary Conditions for Euler Equation Calculations," *AIAA Journal*, Vol. 28, No. 12, December 1990, pp. 2050–2058.

[7] Hall, K. C., Lorence, C. B., and Clark, W. S., "Nonreflecting Boundary Conditions for Linearized Unsteady Aerodynamic Calculations," Paper 93-0882, AIAA 31st Aerospace Sciences Meeting, Reno, NV, January 1993.

[8] Pridmore-Brown, D. C., "Sound Propagation in a Fluid Flowing through an Attenuating Duct," *Journal of Fluid Mechanics*, Vol. 4, 1958, pp. 393–406.

[9] Mungur, P. and Plumblee, H. E., "Propagation and Attenuation of Sound in a Soft-Walled Annular Duct Containing a Sheared Flow," SP 207, NASA, 1969.

[10] Shankar, P. N., "Acoustic Refraction and Attenuation in Cylindrical and Annular Ducts," *Journal of Sound and Vibration*, Vol. 22, No. 2, 1972, pp. 233–246.

[11] Ko, S.-H., "Theoretical Prediction of Sound Attenuation in Acoustically Lined Annular Ducts in the Presence of Uniform Flow and Shear Flow," *Journal of the Acoustical Society of America*, Vol. 54, No. 6, 1973, pp. 1592–1606.

[12] Unruh, J. F. and Eversman, W., "The Transmission of Sound in an Acoustically Treated Rectangular Duct with Boundary Layer," *Journal of Sound and Vibration*, Vol. 25, No. 3, December 1972, pp. 371–382.

[13] Nayfeh, A. H., Kaiser, J. E., and Telionis, D. P., "Acoustics of Aircraft Engine-Duct Systems," *AIAA Journal*, Vol. 13, No. 2, February 1975, pp. 130–153.

[14] Yurkovich, R. N., "Attenuation of Acoustic Modes in Circular and Annular Ducts in the Presence of Sheared Flow," Paper 75–131, AIAA 13th Aerospace Sciences Meeting, Pasadena, CA, January 1975.

[15] Vo, P. T. and Eversman, W., "A Method of Weighted Residuals with Trigonometric Basis Functions for Sound Transmission in Circular Ducts," *Journal of Sound and Vibration*, Vol. 56, No. 2, 1978, pp. 243–250.

[16] Goldstein, M. E., "Characteristics of the Unsteady Motion on Transversely Sheared Mean Flows," *Journal of Fluid Mechanics*, Vol. 84, No. 2, 1978, pp. 305–329.

[17] Goldstein, M. E., "Scattering and Distortion of the Unsteady Motion on Transversely Sheared Mean Flows," *Journal of Fluid Mechanics*, Vol. 91, No. 4, 1979, pp. 601–632.

[18] Greenspan, H. P., *The Theory of Rotating Fluids.* Cambridge University Press, London, 1968.

[19] Kapur, A. and Mungur, P., "Sound Interaction with a Helical Flow Contained in an Annular Duct with Radial Gradients of Flow, Density and Temperature," Paper 73–1010, AIAA Aero-Acoustics Conference, Seattle, WA, October 1973.

[20] Kerrebrock, J. L., "Waves and Wakes in Turbomachine Annuli with Swirl," Paper 74–87, AIAA 12th Aerospace Sciences Meeting, Washington, D.C., January 1974.

[21] Kerrebrock, J. L., "Small Disturbances in Turbomachine Annuli with Swirl," Report 125, MIT GTL, 1975.

[22] Salant, R. F., "Symmetric Normal Modes in a Uniformly Rotating Fluid," *Journal of the Acoustical Society of America*, Vol. 43, No. 6, 1968, pp. 1302–1305.

[23] Yurkovich, R. N., "Attenuation of Acoustic Modes in Circular and Annular Ducts in the Presence of Sheared Swirling Flow," Paper 76–498, AIAA 3rd Aero-Acoustics Conference, Palo Alto, CA, July 1976.

[24] Yousefian, V. *Propagation of Disturbances in Compressor Annuli with Solid Body Rotation and Throughflow.* PhD thesis, Massachusetts Institute of Technology, Cambridge, MA, June 1975.

[25] Wundrow, D. W., "Small-Amplitude Disturbances in Turbomachine Flows with Swirl," Contractor Report 195406, NASA, 1994.

[26] Shankar, P. N., "Sound Propagation in Duct Shear Layers," *Journal of Sound and Vibration*, Vol. 22, No. 2, 1972, pp. 221–232.

[27] Swinbanks, M. A., "The Sound Field Generated by a Source Distribution in a Long Duct Carrying Sheared Flow," *Journal of Sound and Vibration*, Vol. 40, No. 1, 1975, pp. 51–76.

[28] Case, K. M., "Stability of Inviscid Plane Couette Flow," *The Physics of Fluids*, Vol. 3, No. 2, March-April 1960, pp. 143–148.

[29] Case, K. M., "Stability of an Idealized Atmosphere, I: Discussion of Results," *The Physics of Fluids*, Vol. 3, No. 2, March-April 1960, pp. 149–154.

[30] Rayleigh, L. J. W. S., *Scientific Papers*, Vol. VI. Dover Publications, Inc., 1964, Reprint from *Philosophical Magazine*, Vol. XXVI, pp. 1001–1010, 1913.

[31] Goldstein, M. E., "Unsteady Vortical and Entropic Distortions of Potential Flows Round Arbitrary Obstacles," *Journal of Fluid Mechanics*, Vol. 89, 1978, pp. 433–468.

[32] Goldstein, M. E., *Aeroacoustics.* McGraw-Hill International Book Company, New York, 1976.

[33] Canuto, C., Hussaini, M. Y., Quarteroni, A., and Zang, T. A., *Spectral Methods in Fluid Dynamics.* Springer-Verlag, New York, NY, 1978.

[34] Don, W. S. and Solomonoff, A., "Accuracy and Speed in Computing the Chebyshev Collocation Derivative," CR 4411, NASA, 1991.

[35] Don, W. S. and Solomonoff, A., "Accuracy Enhancement for Higher Derivatives Using Chebyshev Collocation and a Mapping Technique," IMA Preprint Series 1236, Institute for Mathematics and its Applications, 1994.

[36] Kosloff, D. and Tal-Ezer, H., "Modified Chebyshev Pseudospectral Methods with $O(N^{-1})$ Time Step Restriction," *Journal of Computational Physics*, Vol. 104, No. 2, 1993, pp. 457–469.

[37] Bayliss, A., Class, A., and Matkowsky, B. J., "Roundoff Error in Computing Derivatives Using the Chebyshev Differentiation Matrix," *Journal of Computational Physics*, Vol. 116, 1994, pp. 380–383.

[38] Gary, J., "On Boundary Conditions for Hyperbolic Difference Schemes," *Journal of Computational Physics*, Vol. 26, No. 3, March 1978, pp. 339–351.

[39] Carpenter, M. H., Gottlieb, D., and Abarbanel, S., "The Stability of Numerical Boundary Treatments for Compact High-Order Finite-Difference Schemes," *Journal of Computational Physics*, Vol. 108, No. 2, October 1993, pp. 272–295.

[40] Anderson, E. e. a., *LAPACK Users' Guide.* Society for Industrial and Applied Mathematics, Philadelphia, PA, 1992.

[41] Strang, G., *Introduction to Applied Mathematics.* Wellesley-Cambridge Press, Wellesley, MA, 1986.

[42] Wu, C. Y., Didwania, A. K., and Goddard, J. D., "Experimental Observations and Marginal Stability Calculations for Counterflowing Streams with Swirl," *Physics of Fluids A*, Vol. 6, No. 4, April 1994, pp. 1464–1471.

[43] Press, W. H., e. a., *Numerical Recipes: The Art of Scientific Computing.* Cambridge University Press, New York, NY, 1989.

[44] Kerrebrock, J. L., *Aircraft Engines and Gas Turbines.* The MIT Press, Cambridge, MA, 1977.

[45] Astley, R. J. and Eversman, W., "A Finite Element Formulation of the Eigenvalue Problem in Lined Ducts with Flow," *Journal of Sound and Vibration*, Vol. 65, No. 1, 1979, pp. 61–74.

[46] Agarwal, N. K. and Bull, M. K., "Acoustic Wave Propagation in a Pipe with Fully Developed Turbulent Flow," *Journal of Sound and Vibration*, Vol. 132, No. 2, 1989, pp. 275–298.

[47] Lin, C. C., *The Theory of Hydrodynamic Stability.* Cambridge University Press, New York, NY, 1967.

[48] Betchov, R. and Criminale, W.O., J., *Stability of Parallel Flows.* Academic Press, New York, NY, 1967.

[49] Chandrasekhar, S., *Hydrodynamic and Hydromagnetic Stability.* Oxford University Press, New York, NY, 1961, (Reprint by Dover Publications, 1981).

[50] Briggs, R. J., *Electron Stream Interaction with Plasmas*, Vol. Massachusetts Institute of Technology Research Monograph No. 29. MIT Press, Cambridge, MA, 1964.

[51] Tam, C. K. W. and Hu, F. Q., "The Instability and Acoustic Wave Modes of Supersonic Mixing Layers Inside a Rectangular Channel," *Journal of Fluid Mechanics*, Vol. 203, 1989, pp. 51–76.

[52] Hu, F. Q., "The Acoustic and Instability Waves of a Jet Confined Inside Acoustically Lined Rectangular Ducts," Paper 93–4350, AIAA 15th Aeroacoustics Conference, Long Beach, CA, October 1993.

[53] Tan, C. S., "Three-Dimensional Incompressible and Compressible Beltrami Flow Through A Highly-Loaded Isolated Rotor," Report No. 147, MIT Gas Turbine & Plasma Dynamics Laboratory, October 1979.

[54] Tan, C. S., "Asymmetric Inlet Flows Through Axial Compressors," Report No. 151, MIT Gas Turbine & Plasma Dynamics Laboratory, January 1980.

[55] Tan, C. S. and Greitzer, E. M., "Nonaxisymmetric Compressible Swirling Flow in Turbomachine Annuli," *AIAA Journal*, Vol. 24, No. 1, January 1986, pp. 92–100.

[56] Harten, A., "On the Symmetric Form of Systems of Conservation Laws with Entropy," Report No. 81-34, ICASE, October 1981.

REPORT DOCUMENTATION PAGE

Form Approved
OMB No. 0704-0188

1. AGENCY USE ONLY (*Leave blank*)	2. REPORT DATE	3. REPORT TYPE AND DATES COVERED
	March 1999	Final Contractor Report

4. TITLE AND SUBTITLE

Eigenmodes of Ducted Flows With Radially-Dependent Axial and Swirl Velocity Components

5. FUNDING NUMBERS

WU–538–03–11–00
NAS3–26618

6. AUTHOR(S)

Kenneth A. Kousen

7. PERFORMING ORGANIZATION NAME(S) AND ADDRESS(ES)

United Technologies Research Center
400 Main Street
East Hartford, Connecticut 06108

8. PERFORMING ORGANIZATION REPORT NUMBER

E–11611

9. SPONSORING/MONITORING AGENCY NAME(S) AND ADDRESS(ES)

National Aeronautics and Space Administration
John H. Glenn Research Center at Lewis Field
Cleveland, Ohio 44135–3191

10. SPONSORING/MONITORING AGENCY REPORT NUMBER

NASA CR—1999-208881
PWA 6420–108

11. SUPPLEMENTARY NOTES

Project Manager, Dennis L. Huff, NASA Lewis Research Center, organization code 5940, (216) 433–3913.

12a. DISTRIBUTION/AVAILABILITY STATEMENT

Unclassified - Unlimited
Subject Category: 71 Distribution: Nonstandard

This publication is available from the NASA Center for AeroSpace Information, (301) 621–0390.

12b. DISTRIBUTION CODE

13. ABSTRACT (*Maximum 200 words*)

This report characterizes the sets of small disturbances possible in cylindrical and annular ducts with mean flow whose axial and tangential components vary arbitrarily with radius. The linearized equations of motion are presented and discussed, and then exponential forms for the axial, circumferential, and time dependencies of any unsteady disturbances are assumed. The resultant equations form a generalized eigenvalue problem, the solution of which yields the axial wavenumbers and radial mode shapes of the unsteady disturbances. Two numerical discretizations are applied to the system of equations: (1) a spectral collocation technique based on Chebyshev polynomial expansions on the Gauss-Lobatto points, and (2) second and fourth order finite differences on uniform grids. The discretized equations are solved using a standard eigensystem package employing the QR algorithm. The eigenvalues fall into two primary categories: a discrete set (analogous to the acoustic modes found in uniform mean flows) and a continuous band (analogous to convected disturbances in uniform mean flows) where the phase velocities of the disturbances correspond to the local mean flow velocities. Sample mode shapes and eigensystem distributions are presented for both sheared axial and swirling flows. The physics of swirling flows is examined with reference to hydrodynamic stability and completeness of the eigensystem expansions. The effect of assuming exponential dependence in the axial direction is discussed.

14. SUBJECT TERMS

Acoustics; Turbomachinery; Noise fans

15. NUMBER OF PAGES

44

16. PRICE CODE

A03

17. SECURITY CLASSIFICATION OF REPORT	18. SECURITY CLASSIFICATION OF THIS PAGE	19. SECURITY CLASSIFICATION OF ABSTRACT	20. LIMITATION OF ABSTRACT
Unclassified	Unclassified	Unclassified	